

Spherical Flows for Sampling Categorical Data

Jannis Chemseddine*
Technische Universität Berlin
chemseddine@math.tu-berlin.de

Gregor Kornhardt
Technische Universität Berlin
kornhardt@math.tu-berlin.de

Gabriele Steidl
Technische Universität Berlin
steidl@math.tu-berlin.de

Abstract

We study the problem of learning generative models for discrete sequences in a continuous embedding space. Whereas prior approaches typically operate in Euclidean space or on the probability simplex, we instead work on the sphere \mathbb{S}^{d-1} . There the von Mises-Fisher (vMF) distribution induces a natural noise process and admits a closed-form conditional score. The conditional velocity is in general intractable. Exploiting the radial symmetry of the vMF density we reduce the continuity equation on \mathbb{S}^{d-1} to a scalar ODE in the cosine similarity, whose unique bounded solution determines the velocity. The marginal velocity and marginal score on $(\mathbb{S}^{d-1})^L$ both decompose into posterior-weighted tangent sums that differ only by per-token scalar weights. This gives access to both ODE and predictor-corrector (PC) sampling. The posterior is the only learned object, trained by a cross-entropy loss. Experiments compare the vMF path against geodesic and Euclidean alternatives. The combination of vMF and PC sampling significantly improves results on Sudoku and language modeling.

1 Introduction

Large language models (LLMs) based on autoregressive decoding are the prevailing approach to text generation. An alternative to sequential generation is to apply diffusion or flow-based generative modeling to produce the entire sequence at once. Such methods have proven remarkably successful for image generation, e.g. Song et al. (2021); Lipman et al. (2023); Geng et al. (2025). Several works extend these methods to discrete data, such as text. As in the continuous setting, a forward process progressively corrupts an entire sequence and generation proceeds by learning to reverse this corruption.

The existing methods can be split into two families. *Discrete diffusion models* Austin et al. (2023); Campbell et al. (2022); Lou et al. (2024); Sahoo et al. (2024) operate directly on the finite state space, corrupting tokens by e.g. masking or replacing them according to a discrete Markov process. *Continuous diffusion methods* instead embed tokens in a continuous space and define the noise process there. For example, Continuous

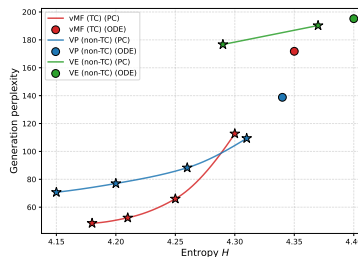


Figure 1: LM1B: Generation perplexity (gen PPL) vs. entropy H at NFE=128 from Table 8 with varying the predictor-to-corrector ratio. Predictor-corrector sampling (stars) outperforms ODE sampling (circles) with a tradeoff between entropy and generation perplexity when using more corrector steps. (non-)TC: (non-)time-conditioned network.

*Corresponding author.

Diffusion for Categorical Data (CDCD) Dieleman et al. (2022) adds Gaussian noise to learned embeddings in \mathbb{R}^d .

In CDCD Dieleman et al. (2022), the token embeddings w_k are normalized to unit norm. The model produces a vector per position and predicts token probabilities via softmax of inner products with the w_k . This output decomposes into a direction on \mathbb{S}^{d-1} and a magnitude. The direction determines the most likely token. The magnitude controls confidence.

In this paper, we propose a continuous noise process directly on \mathbb{S}^{d-1} . We assign each token from a vocabulary a learned embedding w_k on the unit sphere \mathbb{S}^{d-1} . Given a target sequence, a forward process corrupts each position independently by moving the embedding toward a reference distribution on \mathbb{S}^{d-1} . Generation reverses this process by integrating a velocity field on the product manifold $(\mathbb{S}^{d-1})^L$.

What remains to specify is the conditional path $p_t(\cdot|w_k)$ at each position, which determines the marginal flow on $(\mathbb{S}^{d-1})^L$. Two conditional paths arise naturally on the sphere. The first is the geodesic interpolation, the analogue of linear interpolation in \mathbb{R}^d Chen & Lipman (2024). We propose a new one based on the von Mises–Fisher (vMF) family of distributions on \mathbb{S}^{d-1} indexed by a concentration parameter κ .

The vMF density $\varphi(x; w, \kappa) \propto \exp(\kappa \langle w, x \rangle)$ around mean $w \in \mathbb{S}^{d-1}$ with concentration $\kappa \geq 0$ is radially symmetric and depends on x only through the cosine similarity $\langle w, x \rangle$. While the Riemannian score follows directly from this form, the velocity must be derived from the continuity equation. We show that radial symmetry reduces the continuity equation of the vMF path on \mathbb{S}^{d-1} to a scalar ODE in the cosine similarity (Theorem 3.5). The solution of this ODE can be precomputed efficiently. Having both velocity and score in tractable form, the marginal velocity and the marginal score on $(\mathbb{S}^{d-1})^L$ decompose into per-position sums over the vocabulary weighted by the per-position posteriors $p_t^i(w_k|\mathbf{x})$. The minimizer of the per-position cross-entropy loss is precisely this posterior (Proposition 4.1). The learned posteriors therefore determine both the velocity for ODE sampling and the score for predictor-corrector (PC) and SDE sampling.

We validate our method on Sudoku-Extreme and on LM1B for language modeling. In Figure 1, we compare generation perplexity on the LM1B dataset for the vMF path against the baselines, using both the Euler and predictor-corrector samplers.

Contributions. 1. For radially symmetric conditional paths on \mathbb{S}^{d-1} , the continuity equation reduces to a one-dimensional flux equation in the cosine similarity (Theorem 3.2). Applied to the vMF family, this yields the conditional velocity as the unique bounded solution of a scalar ODE (Theorem 3.5). The solution factorizes as $\psi_t = \hat{\kappa}_t \tilde{\psi}_t$, where $\tilde{\psi}_t$ is schedule-independent and admits a numerically stable evaluation (Remark 3.6).

2. We build a generative model on $(\mathbb{S}^{d-1})^L$ using both geodesic and vMF conditional paths. The per-position cross-entropy loss trains the model to output the marginal posteriors (Proposition 4.1). For the vMF path these posteriors determine the marginal velocity and the Riemannian score, giving access to ODE, SDE, and predictor-corrector sampling from a single model.

3. We evaluate the models on a challenging Sudoku dataset and LM1B, comparing vMF and geodesic spherical paths against Euclidean baselines. The Riemannian score enables predictor-corrector sampling that substantially improves over ODE sampling, especially for vMF flows.

For related work see Section 6. All proofs are in Appendix A.

2 Background: Continuous Flows for Discrete Data

To sample from a discrete data distribution p_{data} via flow-based generation, we embed the discrete data into a continuous Riemannian manifold and construct a flow of measures. It has been shown, for example in Lee et al. (2026), that for discrete data it is often advantageous to train a denoiser $p_1(\cdot|\mathbf{x})$ with a cross-entropy loss. We therefore use the standard decomposition of the velocity as a conditional expectation, obtained by the law of total probability. We recall this construction here. The choice of manifold and conditional path is deferred to Section 3.

2.1 Setting and Continuous Embedding

Let $\mathcal{V} := \{v_1, \dots, v_N\}$ be a vocabulary of tokens and $(\Omega, \mathcal{A}, \mathbb{P})$ a probability space. Our aim is to sample from a discrete random variable $\mathbf{Y} = (Y^1, \dots, Y^L) : \Omega \rightarrow \mathcal{V}^L$ given training samples. For the concrete choice of N and L , see Section 5.

To apply flow-based generative modeling, we embed \mathcal{V} into a Riemannian manifold

$$\mathcal{M} \in \{\mathbb{R}^d, \mathbb{S}^{d-1}\}, \quad d > 1,$$

and operate on its L -fold product \mathcal{M}^L . We work with extrinsic representations on \mathbb{S}^{d-1} , viewing its points as elements of \mathbb{R}^d of unit norm. All norms and inner products in this paper are inherited from \mathbb{R}^d . The constructions below extend to general finite-dimensional smooth Riemannian manifolds, see Ambrosio & Trevisan (2014); Villani (2008).

Embedding and decoding. To each token $v_k \in \mathcal{V}$ we assign an element $w_k \in \mathcal{M}$, collected into $\mathcal{W} := \{w_1, \dots, w_N\} \subset \mathcal{M}$. This induces a token-wise embedding $W_E : \mathcal{V}^L \rightarrow \mathcal{M}^L$ defined by $W_E(\mathbf{y})^l := w_{y^l}$, for $\mathbf{y} \in \mathcal{V}^L$. The distribution induced by applying W_E to \mathbf{Y} is a \mathcal{W}^L -valued random variable \mathbf{W} with probability mass function (pmf)

$$p_{\text{data}}(\mathbf{w}) := \mathbb{P}(\mathbf{W} = \mathbf{w}),$$

and this is the distribution we aim to sample from. The embeddings $\{w_k\}$ will be learnable parameters of the model, optimized jointly with the network in Section 4. To return token sequences, we equip the model with a decoder that maps a generated state on \mathcal{M}^L back to \mathcal{V}^L . The specific decoder we use is defined in Section 4.

2.2 Conditional Flows of Measures

We sample from p_{data} by constructing a flow of measures from a simple noise distribution to the data distribution. The standard machinery is summarized below, for details see Albergo et al. (2025); Chen & Lipman (2024); Wald & Steidl (2025).

Measure Flows. Let $p_t : I \rightarrow \mathcal{P}(\mathcal{M})$ be a curve of probability densities on \mathcal{M} (with respect to the Riemannian volume measure) for $I = (0, 1)$, and let $v : I \times \mathcal{M} \rightarrow \mathcal{T}\mathcal{M}$ be a sufficiently smooth Borel-measurable vector field. The pair (p_t, v_t) satisfies the *continuity equation*

$$\partial_t p_t + \text{div}_{\mathcal{M}}(p_t v_t) = 0 \tag{CE}$$

if and only if there exists a solution $\Phi : I \times \mathcal{M} \rightarrow \mathcal{M}$ of the *flow ODE*

$$\partial_t \Phi(t, x) = v_t(\Phi(t, x)), \quad \Phi(0, x) = x, \tag{Flow ODE}$$

with $p_t = \Phi(t, \cdot)_{\#} p_0$. We can therefore sample from p_1 by drawing $x \sim p_0$ and integrating (Flow ODE) numerically up to $t = 1$.

The same flow of measures admits a stochastic realization once the score $\nabla_{\mathcal{M}} \log p_t$ is available, which we defer to Appendix B. The differential operators $\nabla_{\mathcal{M}}, \text{div}_{\mathcal{M}}, \Delta_{\mathcal{M}}$ for $\mathcal{M} = \mathbb{S}^{d-1}$ are recalled in Section 3.

For paths of measures on the product manifold \mathcal{M}^L , we construct (p_t, v_t) in three steps: a conditional flow on \mathcal{M} , its product on \mathcal{M}^L , and the marginal flow obtained from p_{data} .

1. Conditional Flows on \mathcal{M} . Fix a position $l \in \{1, \dots, L\}$ and drop the superscript, writing $W : \Omega \rightarrow \mathcal{W}$ for W^l . Let $p_0 \in \mathcal{P}(\mathcal{M})$ be easy to sample from (for instance, the standard Gaussian on \mathbb{R}^d or the uniform measure on \mathbb{S}^{d-1}), and $Z \sim p_0$. For each fixed $w \in \mathcal{W}$, we suppose we can construct a path of conditional random variables $X_t \mid W = w, t \in [0, 1]$, between Z and δ_w , with conditional densities $p_t(x \mid w)$ and velocity fields $v_t(x \mid w)$ fulfilling the conditional continuity equation

$$\partial_t p_t(x \mid w) + \text{div}_{\mathcal{M}}(p_t(x \mid w) v_t(x \mid w)) = 0, \quad t \in (0, 1). \tag{1}$$

This is the design choice of the method. We give two natural choices on \mathbb{S}^{d-1} in Section 3. For now, the standard \mathbb{R}^d example serves as a reference.

Example 2.1 (Linear interpolation on \mathbb{R}^d). For $\mathcal{M} = \mathbb{R}^d$, the linear interpolation path $X_t \mid W = w := tw + (1-t)Z$ with $Z \sim \mathcal{N}(0, \mathbf{I}_d)$ has conditional density $p_t(x \mid w) = \mathcal{N}(x; tw, (1-t)^2 \mathbf{I}_d)$ and velocity $v_t(x \mid w) = (w - x)/(1-t)$, which fulfill (1) with $p_0(x \mid w) = \mathcal{N}(x; 0, \mathbf{I}_d)$.

2. Conditional Flows on \mathcal{M}^L . Conditional flows on single positions combine into a conditional flow on \mathcal{M}^L by taking products.

Proposition 2.2. *Let $\mathbf{w} = (w^l)_{l=1}^L \in \mathcal{W}^L$ be fixed, and let $p_t^l(\cdot | w^l)$ be absolutely continuous measures on \mathcal{M} with velocities $v_t^l(\cdot | w^l)$ satisfying the conditional continuity equation (1) on \mathcal{M} for each $l = 1, \dots, L$. Then the product density on \mathcal{M}^L ,*

$$p_t(\mathbf{x} | \mathbf{w}) = \prod_{l=1}^L p_t^l(x^l | w^l), \quad \mathbf{x} = (x^1, \dots, x^L), \quad (2)$$

with the velocity field $v_t(\mathbf{x} | \mathbf{w}) := (v_t^1(x^1 | w^1), \dots, v_t^L(x^L | w^L))$ satisfies the continuity equation on \mathcal{M}^L for $t \in (0, 1)$.

The proof is given in Appendix A. Related factorization results appear in the generator-matching framework Holderrieth et al. (2025) and in discrete flow matching Lipman et al. (2024), for general measures, see Chemseddine et al. (2026); Duong et al. (2026).

3. Marginal Flow on \mathcal{M}^L . By the law of total probability, the unconditional density on \mathcal{M}^L at time t is

$$p_t(\mathbf{x}) = \sum_{\mathbf{w} \in \mathcal{W}^L} p_t(\mathbf{x} | \mathbf{w}) p_{\text{data}}(\mathbf{w}), \quad (3)$$

which interpolates between p_0 and p_{data} as t goes from 0 to 1. Direct evaluation is intractable since p_{data} is unknown. The associated marginal velocity

$$v_t(\mathbf{x}) = \sum_{\mathbf{w} \in \mathcal{W}^L} v_t(\mathbf{x} | \mathbf{w}) p_t(\mathbf{w} | \mathbf{x}), \quad p_t(\mathbf{w} | \mathbf{x}) = p_t(\mathbf{x} | \mathbf{w}) \frac{p_{\text{data}}(\mathbf{w})}{p_t(\mathbf{x})}, \quad (4)$$

fulfills the continuity equation (CE) on \mathcal{M}^L Wald & Steidl (2025). By (2), its components $v_t = (v_t^l)_{l=1}^L$ simplify by marginalization to

$$\begin{aligned} v_t^l(\mathbf{x}) &= \sum_{\mathbf{w} \in \mathcal{W}^L} v_t^l(x^l | w^l) p_t(\mathbf{w} | \mathbf{x}) = \sum_{w^l \in \mathcal{W}} v_t^l(x^l | w^l) \sum_{\substack{\mathbf{w} \in \mathcal{W}^L \\ \mathbf{w}^l = w^l}} p_t(\mathbf{w} | \mathbf{x}) \\ &= \sum_{w^l \in \mathcal{W}} v_t^l(x^l | w^l) p_t^l(w^l | \mathbf{x}), \end{aligned}$$

where we group sequences $\mathbf{w} \in \mathcal{W}^L$ by their l -th component, with w^l first denoting that fixed l -th component and then ranging over \mathcal{W} in the outer sum. The same per-position reduction applies to the score. Differentiating (3) with respect to x^l , only the l -th factor of $p_t(\mathbf{x} | \mathbf{w})$ in (2) contributes, so

$$\nabla_{\mathcal{M}, x^l} \log p_t(\mathbf{x}) = \sum_{w^l \in \mathcal{W}} \nabla_{\mathcal{M}, x^l} \log p_t^l(x^l | w^l) p_t^l(w^l | \mathbf{x}). \quad (5)$$

Example 2.3. *Continuing Example 2.1 with $\mathcal{M}^L = \mathbb{R}^{Ld}$, the path*

$$\mathbf{X}_t = t\mathbf{W} + (1-t)\mathbf{Z}, \quad \mathbf{Z} \sim \mathcal{N}(0, \mathbf{I}_{Ld})$$

has laws (3). The components of the corresponding vector field (4) read as

$$v_t^l(\mathbf{x}) = \sum_{w^l \in \mathcal{W}} \frac{w^l - x^l}{1-t} p_t^l(w^l | \mathbf{x}).$$

The conditional density $p_t^l(\cdot | w^l) = \mathcal{N}(\cdot, tw^l, (1-t)^2 \mathbf{I}_d)$ has score

$$\nabla_{x^l} \log p_t^l(x^l | w^l) = \frac{tw^l - x^l}{(1-t)^2}.$$

Substituting into (5), the score of the unconditional density at position l is

$$\nabla_{x^l} \log p_t(\mathbf{x}) = \frac{1}{(1-t)^2} \left(t \sum_{w^l \in \mathcal{W}} p_t^l(w^l | \mathbf{x}) w^l - x^l \right).$$

The posterior is the only learned object. In summary, both the velocity field (4) and the score (5) of the unconditional density are weighted sums over \mathcal{W} with the same marginal conditional pmfs $p_t^l(w^l|\mathbf{x})$. The conditional quantities $v_t^l(x^l|w^l)$ and $\nabla_{x^l} \log p_t^l(x^l|w^l)$ are determined by the choice of noise process. The marginal posteriors $p_t^l(w^l|\mathbf{x})$ must be learned.

What remains to specify is the conditional path $p_t(\cdot | w)$ on \mathcal{M} . In Section 3, we work on $\mathcal{M} = \mathbb{S}^{d-1}$ and consider two natural choices: geodesic interpolation and a path through the von Mises-Fisher family. The latter yields a tractable conditional velocity via a radial-symmetry reduction and an informative range that scales correctly with the embedding dimension.

3 Conditional von Mises-Fisher Paths

So far, we have only given concrete examples for $v_t^l(x^l|w^l)$ on $\mathcal{M} = \mathbb{R}^d$. Assuming that the weights w_k are normalized, i.e. $\|w_k\| = 1, k = 1, \dots, N$, the target embeddings live on the $(d-1)$ -sphere, with $d > 1$. We propose to use a path of measures that stays on this manifold.

3.1 Background on the Sphere

Differential operators. For the sphere $\mathbb{S}^{d-1} := \{x \in \mathbb{R}^d : \|x\| = 1\}$, the geodesic distance between two points $x, z \in \mathbb{S}^{d-1}$ is given by $d(x, z) := \theta = \arccos(\langle x, z \rangle)$. The tangent space at a point $x \in \mathbb{S}^{d-1}$ is

$$\mathcal{T}_x \mathbb{S}^{d-1} = \{v \in \mathbb{R}^d : \langle v, x \rangle = 0\}$$

and the orthogonal projection onto $\mathcal{T}_x \mathbb{S}^{d-1}$ reads as

$$P_x(w) := w - \langle w, x \rangle x, \quad w \in \mathbb{R}^d.$$

Let $\tilde{g} : \mathbb{R}^d \rightarrow \mathbb{R}$ be sufficiently smooth and $g = \tilde{g}|_{\mathbb{S}^{d-1}}$. Then the Riemannian gradient of g on \mathbb{S}^{d-1} is the orthogonal projection of the Euclidean gradient ∇g onto $\mathcal{T}_x \mathbb{S}^{d-1}$, i.e.,

$$\nabla_{\mathbb{S}^{d-1}} g(x) = P_x(\nabla \tilde{g}(x)) = \nabla \tilde{g}(x) - \langle \nabla \tilde{g}(x), x \rangle x.$$

For a differentiable vector field $\tilde{u} : \mathbb{R}^d \rightarrow \mathbb{R}^d$ and $u = \tilde{u}|_{\mathbb{S}^{d-1}}$, the divergence is defined by

$$\operatorname{div}_{\mathbb{S}^{d-1}} u(x) = \operatorname{tr}(\nabla \tilde{u}(x)) - x^\top \nabla \tilde{u}(x) x$$

and the Laplace-Beltrami operator becomes

$$\Delta_{\mathbb{S}^{d-1}} g(x) = \operatorname{tr}((I_d - xx^\top) \nabla^2 \tilde{g}(x)) - (d-1) \langle \nabla \tilde{g}(x), x \rangle.$$

In the rest of this paper, we always assume that functions, resp. vector fields on the $(d-1)$ -sphere have a smooth extension to functions, resp. vector fields living in the whole \mathbb{R}^d and we skip the 'tilde'.

Remark 3.1 (Geodesic Path). *Using the geodesic between two points, one can construct the slerp path*

$$X_t = \frac{\sin((1-t)\theta)}{\sin \theta} X_0 + \frac{\sin(t\theta)}{\sin \theta} X_1, \quad t \in [0, 1], \quad (6)$$

where $\theta := \arccos(\langle X_0, X_1 \rangle)$, $X_0 \sim \mathcal{U}(\mathbb{S}^{d-1})$. With the linear interpolation on \mathbb{R}^d from Examples 2.1 and 2.3 in mind, this is its spherical counterpart. This path is sometimes called spherical linear interpolation (**slerp**). Using this path for generative modeling via flows is a straightforward application of Riemannian Flow Matching Chen & Lipman (2024).

In this paper, we propose another path based on special radially symmetric functions on the sphere.

Radial symmetry on the sphere. A function $p : \mathbb{S}^{d-1} \rightarrow \mathbb{R}_{\geq 0}$ is called *radially symmetric around* $w \in \mathbb{S}^{d-1}$, if there exists a function $\bar{p} : [-1, 1] \rightarrow \mathbb{R}$ such that

$$p(x) = \bar{p}(\langle w, x \rangle) \quad \text{for all } x \in \mathbb{S}^{d-1}.$$

Note that $|\langle w, x \rangle| \leq \|w\| \|x\| = 1$ with equality iff $x = w$. Extending \bar{p} to the whole \mathbb{R} , the map $x \mapsto p(\langle w, x \rangle)$ extends to all of \mathbb{R}^d and

$$\nabla_{\mathbb{S}^{d-1}} p(x) = P_x(\bar{p}'(\langle w, x \rangle) w) = \bar{p}'(\langle w, x \rangle) P_x(w).$$

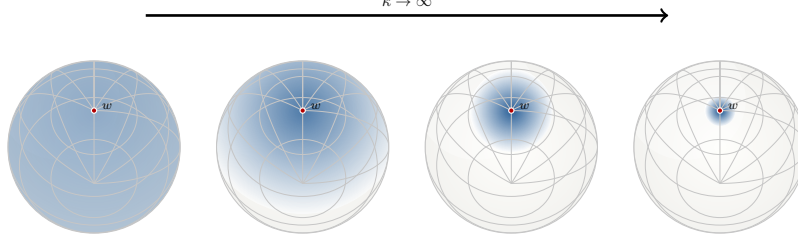


Figure 2: Illustration of von Mises–Fisher density on \mathbb{S}^2 for increasing concentration κ . At $\kappa = 0$ (left) the density is uniform. As κ grows the mass concentrates around the mean direction w , collapsing to a point mass at w as $\kappa \rightarrow \infty$.

A tangent vector field $v : \mathbb{S}^{d-1} \rightarrow \mathcal{T}_x \mathbb{S}^{d-1}$ is *radially symmetric around* $w \in \mathbb{S}^{d-1}$, if there exists $\psi : [-1, 1] \rightarrow \mathbb{R}$ such that

$$v(x) = \psi(\langle w, x \rangle) P_x(w).$$

Given a random variable X with radially symmetric density p around w , the random variable $S = w^\top X \in [-1, 1]$ has the density $C f$ with

$$f(s) := (1 - s^2)^{(d-3)/2} \bar{p}(s), \quad s \in (-1, 1), \quad (7)$$

and normalizing factor C . In particular, we have for $d = 3$ that $f = \bar{p}$. The following theorem shows that the continuity equation of a radially symmetric density on the sphere can be reduced to the one-dimensional flux function on the interval $[-1, 1]$.

Theorem 3.2. *Let (p_t, v_t) , $t \in I$ be a sequence of radially symmetric pairs of densities and velocities of the form $p_t(x) = \bar{p}_t(\langle x, w \rangle)$, resp. $v_t(x) = \psi_t(\langle x, w \rangle) P_x(w)$, where $\bar{p}_t \in C^1[I \times (-1, 1)]$ and $\psi_t \in C^1(-1, 1)$ for every $t \in I$. Let f_t , $t \in I$ be the corresponding densities defined by (7). Then (p_t, v_t) , $t \in I$ satisfy the continuity equation*

$$\partial_t p_t + \operatorname{div}_{\mathbb{S}^{d-1}}(p_t v_t) = 0, \quad t \in I, x \in \mathbb{S}^{d-1} \setminus \{\pm w\} \quad (8)$$

if and only if (f_t, ψ_t) satisfy the one-dimensional flux equation

$$\partial_t f_t + \partial_s (f_t \psi_t \cdot (1 - s^2)) = 0, \quad t \in I, s \in (-1, 1). \quad (9)$$

3.2 von Mises-Fisher Distribution and Path

The *von Mises-Fisher distribution* with mean $w \in \mathbb{S}^{d-1}$ and concentration $\kappa \geq 0$, denoted by $\text{vMF}(w, \kappa)$, has the density

$$\varphi(x; w, \kappa) = C_d(\kappa) \exp(\kappa \langle w, x \rangle), \quad (\text{vMF})$$

where

$$C_d(\kappa) := \kappa^{d/2-1} / ((2\pi)^{d/2} \mathcal{I}_{d/2-1}(\kappa))$$

is the normalization constant and $\mathcal{I}_{d/2-1}$ is the modified Bessel function of the first kind and order $d/2 - 1$. At $\kappa = 0$ the distribution is uniform on \mathbb{S}^{d-1} , and as $\kappa \rightarrow \infty$ it concentrates to a point mass at w , see Figure 2. The normalization constant $C_d(\kappa)$ depends only on κ and not on the mean direction w . The *mean resultant length* of the vMF distribution is the Bessel ratio

$$A_d(\kappa) := \mathbb{E}_{x \sim \text{vMF}(w, \kappa)}[\langle w, x \rangle] = \frac{\mathcal{I}_{d/2}(\kappa)}{\mathcal{I}_{d/2-1}(\kappa)},$$

which is equal to the expected cosine similarity, see (Mardia & Jupp, 2000, Chapter 9). In particular, A_d is strictly monotone increasing, $A_d(0) = 0$, $A_d(\kappa) = \kappa/d + O(\kappa^3)$ as $\kappa \rightarrow 0$ and $A_d(\kappa) \rightarrow 1$ as $\kappa \rightarrow \infty$.

In the following, let $\kappa_t : [0, 1] \rightarrow [0, \infty)$ be a continuously differentiable, strictly monotone increasing schedule function with $\kappa_0 = 0$, which will be specified later. Then we consider, for fixed $w \in \mathcal{W}$, a sequence of random variables $X_t | W = w$ on \mathbb{S}^{d-1} , $t \in [0, 1]$ with laws forming the *conditional vMF path*

$$p_t(\cdot | w) := \varphi(\cdot; w, \kappa_t) = \bar{p}_t(\langle w, \cdot \rangle). \quad (10)$$

Clearly, p_t are radially symmetric functions and the corresponding function f_t in (7) reads as

$$f_t(s) = C_d(\kappa_t) (1 - s^2)^{(d-3)/2} \exp(\kappa_t s), \quad s \in (-1, 1). \quad (11)$$

Lemma 3.3. Let $f_t, t \in I$ be defined by (11). Then $\psi_t, t \in I$ solves the linear ODE

$$(1 - s^2) \psi_t' + (\kappa_t(1 - s^2) - (d - 1)s) \psi_t = (A_d(\kappa_t) - s) \dot{\kappa}_t, \quad s \in (-1, 1) \quad (12)$$

if and only if $(f_t, \psi_t), t \in I$ fulfill the flux equation (9).

We have to deal with the possible singularity of the ODE (12) at $x = \pm 1$. This can be handled similarly as for the Kac process, see e.g. Duong et al. (2026), by the following lemma.

Lemma 3.4. For any $t \in I$, the ODE (12) has a unique solution ψ_t in $C[-1, 1]$, which is automatically also in $C^\infty(-1, 1)$ with boundary values $\psi_t(1) = \frac{(1 - A_d(\kappa_t))\dot{\kappa}_t}{d-1}$, and $\psi_t(-1) = \frac{(1 + A_d(\kappa_t))\dot{\kappa}_t}{d-1}$.

As a direct consequence of Theorem 3.2, Lemma 3.3 and Lemma 3.4, we obtain access to the conditional velocities in our key formula (4) for the vMF path.

Theorem 3.5. Let $p_t(\cdot|w)$ be the conditional vMF path defined by (10) and let $\psi_t, t \in I$ be the unique $C[-1, 1]$ solutions of the ODE (12). Then $p_t(\cdot|w)$ together with the velocities

$$v_t(x|w) = \psi_t(\langle w, x \rangle) P_x(w)$$

fulfill the continuity equation (8) on \mathbb{S}^{d-1} .

Remark 3.6. The conditional velocity in Theorem 3.5 is expressed in terms of ψ_t , which is defined as the unique bounded solution of the ODE (12). For practical computation, we will use the following expression. The proof of Lemma 3.4 uses the integral representation (26). By (11), this can be rewritten as

$$\psi_t(s) = \dot{\kappa}_t \tilde{\psi}_t(s) \quad \text{with} \quad \tilde{\psi}_t(s) := -\frac{\int_{-1}^s (y - A_d(\kappa_t)) f_t(y) dy}{f_t(s) (1 - s^2)}. \quad (13)$$

The function $\tilde{\psi}$ depends only on κ_t and not on the schedule. This representation is both schedule-independent and amenable to numerically stable evaluation, see Section 5 and Section C.3 for the implementation.

The geodesic interpolation from Remark 3.1 and the vMF path from Theorem 3.5 both define conditional paths starting from the uniform distribution on \mathbb{S}^{d-1} . We want to highlight that they differ in how quickly the noisy sample reveals the target with increasing dimension d . We quantify this by comparing the expected cosine similarity under both paths.

Proposition 3.7. Let $X_0 \sim \mathcal{U}(\mathbb{S}^{d-1})$ and $w \in \mathbb{S}^{d-1}$ be arbitrary fixed. Then the conditional geodesic interpolation path (slerp) in (6) fulfill

$$\mathbb{E}_{x_t \sim \text{slerp}_t(x_0, w)}[\langle w, x_t \rangle] \rightarrow \sin\left(\frac{\pi}{2} t\right) \quad \text{as} \quad d \rightarrow \infty, \quad (14)$$

the vMF path (10),

$$\mathbb{E}_{x_t \sim \text{vMF}(w, \kappa_t)}[\langle w, x_t \rangle] = A_d(\kappa_t) = \frac{\kappa_t}{d} + O(\kappa_t^3). \quad (15)$$

Under geodesic interpolation, the expected cosine similarity at any fixed $t > 0$ is bounded away from zero independently of d . Under the vMF path, reaching the same signal level requires κ_t proportional to d . The informative range of the noise parameter therefore grows with d .

4 Generative Model

We now specify how to build a generative model on $(\mathbb{S}^{d-1})^L$ from the conditional paths constructed in Section 2.

4.1 Learning

By (4) and (5), both the velocity field and the score of the unconditional density are determined by the marginal conditional pmfs $p_t^l(w^l|\mathbf{x})$. We learn these pmfs using a neural network.

Let $T_{\theta, t} : \mathcal{M}^L \rightarrow (\mathbb{R}^d)^L, \mathbf{x} \mapsto \hat{\mathbf{x}} := T_{\theta, t}(\mathbf{x})$ be a backbone network. We define a factorized approximation

$$p_{\theta, t}(\mathbf{w}|\mathbf{x}) := \prod_{l=1}^L p_{\theta, t}^l(w^l|\hat{x}^l),$$

where for $w_k \in \mathcal{W}$,

$$p_{\theta,t}^l(w_k|\hat{x}^l) = \frac{\exp(s_k^l)}{\sum_{j=1}^N \exp(s_j^l)}, \quad s_k^l := \langle w_k, \hat{x}^l \rangle + b_k \quad (16)$$

with learnable biases $b_k \in \mathbb{R}$.

Recall that the Kullback–Leibler divergence of two pmfs p, q on a discrete space of size N with $p(k) = 0$ whenever $q(k) = 0$ is $\text{KL}(p||q) = \sum_{k=1}^N (p(k) \log p(k) - p(k) \log q(k))$ and their cross entropy and entropy by $\text{CE}(p, q) = -\sum_{k=1}^N p(k) \log q(k) = \text{KL}(p||q) + \text{H}(p)$, $\text{H}(p) = -\sum_{k=1}^N p(k) \log p(k)$. Since $\text{KL}(p||q) \geq 0$ with equality if and only if $p = q$, the cross entropy $\text{CE}(p, q)$ is minimized in q exactly at $q = p$.

Having this in mind, we train p_θ with the *cross-entropy loss*

$$\mathcal{L}(\theta) = -\mathbb{E}_{t \sim \mathcal{U}(0,1), \mathbf{w} \sim p_{\text{data}}, \mathbf{x}_t \sim p_t(\cdot|\mathbf{w})} \left[\sum_{l=1}^L \log p_{\theta,t}^l(w^l|\mathbf{x}_t) \right]. \quad (17)$$

Proposition 4.1. *The minimizer of (17) is the per-position marginal posterior $p_t^l(\cdot|\mathbf{x})$ from (4).*

A short derivation is given in Appendix A.

The embeddings $\{w_k\}_{k=1}^N$ are learned jointly with θ , with each w_k constrained to \mathbb{S}^{d-1} . Gradients of (17) flow into w_k through the conditional path $p_t(\cdot|w^l)$ and through the decoder logits (16). The pmf p_{data} on \mathcal{W}^L is the pushforward of the fixed law of \mathbf{Y} on \mathcal{V}^L under W_E . For any \mathcal{W} , Proposition 4.1 characterizes the optimal θ .

Remark 4.2 (Noise schedule). *The loss (17) draws $t \sim \mathcal{U}(0, 1)$ uniformly. In practice we replace $\mathcal{U}(0, 1)$ with a learned distribution following CDCD Dieleman et al. (2022). A learnable monotone $\tilde{F} : [0, 1] \rightarrow \mathbb{R}_{\geq 0}$ is fit to the per-sample cross-entropy, and the normalized curve $F = \tilde{F}/\tilde{F}(1)$ serves as a CDF on $[0, 1]$ from which t is drawn by inverse-transform sampling. We use the same scheme for every conditional path in our experiments. Full details are in Appendix C.*

Once the network approximates the per-position marginal posteriors, $p_t^l(\cdot|\mathbf{x}) \approx p_{\theta,t}^l(\cdot|\hat{x}_t^l)$, the marginal velocity (4) and score (5) of the vMF path follow. By Theorem 3.5, the conditional velocity is $v_t(x^l|w) = \psi_t(\langle w, x^l \rangle) P_{x^l}(w)$ and substituting $\psi_t = \dot{\kappa}_t \tilde{\psi}_t$ from (13) into (4), the *marginal velocity at position l* becomes

$$v_{\theta,t}^l(\mathbf{x}) = \dot{\kappa}_t \sum_{k=1}^N p_{\theta,t}^l(w_k|\mathbf{x}) \tilde{\psi}_t(\langle w_k, x^l \rangle) P_{x^l}(w_k). \quad (18)$$

For the conditional score, recall that by (vMF) it holds $\log p_t^l(x^l|w) = \log C_d(\kappa_t) + \kappa_t \langle w, x^l \rangle$. The normalization constant does not depend on x^l . Projecting the Euclidean gradient $\kappa_t w$ onto the tangent space gives $\nabla_{\mathbb{S}^{d-1}} \log p_t^l(x^l|w) = \kappa_t P_{x^l}(w)$. Substituting into (5), the *marginal score at position l* becomes

$$\nabla_{\mathbb{S}^{d-1}, x^l} \log p_{\theta,t}(\mathbf{x}) = \kappa_t \sum_{k=1}^N p_{\theta,t}^l(w_k|\mathbf{x}) P_{x^l}(w_k). \quad (19)$$

Both the marginal velocity and the marginal score at position l are posterior-weighted sums of tangent projections $P_{x^l}(w_k)$, differing only in the scalar weights. The velocity carries the schedule-dependent prefactor $\dot{\kappa}_t \tilde{\psi}_t(\langle w_k, x^l \rangle)$, while the score carries κ_t . In particular, the posteriors $p_{\theta,t}^l(w_k|\mathbf{x})$ are the only learned quantities needed to evaluate velocity, score, and any linear combination of the two.

4.2 Sampling

The pair (p_t, v_t) in (3) and (4) with velocity components (18) satisfies the continuity equation (CE) on $(\mathbb{S}^{d-1})^L$. We focus on ODE sampling and predictor-corrector sampling. The score (19) also makes SDE sampling available, which we outline in Appendix B.

Flow ODE. The associated flow ODE

$$\partial_t \Phi^l(t, \mathbf{x}) = v_t^l(\Phi(t, \mathbf{x})), \quad \Phi^l(0, \mathbf{x}) = x^l \sim \mathcal{U}(\mathbb{S}^{d-1}), \quad l = 1, \dots, L,$$

transports $p_0 \sim \mathcal{U}(\mathbb{S}^{(d-1)L})$ to $p_1 = p_{\text{data}}$. The equations are coupled through the posterior $p_t^l(w_k|\mathbf{x})$, which depends on the full state $\mathbf{x} = (x^1, \dots, x^L)$ via the backbone. Since κ_t is strictly monotone, we discretize the ODE with Euler steps of size $\Delta\kappa_n = \kappa_{t_{n+1}} - \kappa_{t_n}$ in concentration space, using the factorization $\psi_t = \dot{\kappa}_t \hat{\psi}_t$ from (13) so that $\dot{\kappa}_t$ cancels and never appears explicitly. Numerical integration introduces discretization errors that accumulate over steps.

Predictor-corrector. The score provides a mechanism to do corrector steps during inference. After advancing the state by one ODE step, we apply k Langevin diffusion steps at the current concentration κ_t , which leave p_t invariant. The Langevin dynamics on $(\mathbb{S}^{d-1})^L$ read per position as

$$dX_\tau^l = \nabla_{\mathbb{S}^{d-1}, x^l} \log p_t(\mathbf{X}_\tau) d\tau + \sqrt{2} dB_\tau^l = \kappa_t \sum_{k=1}^N p_t^l(w_k|\mathbf{X}_\tau) P_{x^l}(w_k) d\tau + \sqrt{2} dB_\tau^l, \text{ (PC)}$$

where B_τ^l is Brownian motion on \mathbb{S}^{d-1} at position l , independent across positions. The discretization is given in Algorithm 2.

Decoding. Recall from Section 3 that the schedule $\kappa_t : [0, 1] \rightarrow \mathbb{R}_{\geq 0}$ is continuously differentiable and strictly monotone increasing with $\kappa_0 = 0$. We choose a finite terminal concentration $\kappa_{\text{max}} := \kappa_1 > 0$. Sampling consists of solving the flow ODE (Flow ODE) from $t = 0$ to $t = 1$, optionally interleaved with Langevin corrections, transporting the uniform distribution on $(\mathbb{S}^{d-1})^L$ to a terminal density on $(\mathbb{S}^{d-1})^L$. At the terminal state \mathbf{x}_1 , we pass through the backbone to obtain $\hat{\mathbf{x}} = T_\theta(\mathbf{x}_1)$ and decode the token at each position $l \in \{1, \dots, L\}$ as

$$\hat{y}^l = v_{k^*}, \quad k^* := \arg \max_{k=1, \dots, N} s_k^l, \quad s_k^l = \langle w_k, \hat{x}^l \rangle + b_k. \quad (20)$$

5 Experiments

We evaluate the vMF path on Sudoku and the One Billion Word Benchmark Chelba et al. (2013). We compare four continuous conditional paths, two spherical and two Euclidean ones:

1. vMF path (Section 3),
2. slerp geodesic interpolation (Remark 3.1),
3. variance-preserving (VP) i.e the linear interpolation from 2.3, given as $h_t = (1-t)Z + tw_k$ with $Z \sim \mathcal{N}(0, I)$ and
4. variance-exploding (VE), given as $h_t = w_k + \sigma_t Z$ with σ_t growing from 0 to a terminal σ_{max} .

For more details see Appendix C.3.

Sampling ablation. At inference, we run two samplers per method at fixed NFE = 128 network evaluations. The first is an Euler integrator of the flow ODE (Flow ODE) with n predictor steps. The second is the predictor-corrector scheme (PC), in which each predictor step is followed by k Langevin corrector steps, so that NFE = $n(1+k)$. We sweep the predictor-corrector split, predictor spacing, and corrector step size at fixed NFE = 128. Tables 1 and 2 report the best result per cell over the sweep. Full grids, configurations, and the sweep description are in Appendix C.5. Geodesic and masked admit only ODE sampling.

Networks. All continuous methods share a DiT-style transformer Peebles & Xie (2023) backbone with adaLN conditioning. Embeddings are tied to the softmax classifier head as described in Section 4. Masked diffusion uses the same backbone but with a discrete embedding layer of width equal to the hidden size, replacing the tied learned embeddings. The hyperparameters per-task are listed in Table 3.

Method	ODE (%)	PC (%)
<i>Reference</i>		
MDM $_{p=1}$	22.4	–
MDM $_{p=0.5}$	35.1	–
<i>Time-conditioned</i>		
vMF	65.8	74.5
Geodesic	49.4	–
VP	53.4	69.1
VE	48.0	46.5
<i>Non-time-conditioned</i>		
vMF	56.4	78.2
Geodesic	52.2	–
VP	54.8	73.4
VE	53.4	52.3

Table 1: Sudoku validity (\uparrow) under ODE sampling and predictor-corrector sampling. PC reports the best configuration over the full sweep grid (Appendix C.5.2).

5.1 Sudoku

Sudoku is a standard puzzle played on a 9×9 grid, partitioned into nine 3×3 subgrids. Some cells are pre-filled as *clues*, and the goal is to fill the remaining cells with digits 1–9 such that each row, each column, and each 3×3 subgrid contains every digit exactly once.

Setup. We use the Sudoku-Extreme dataset from Wang et al. (2025). Generation is conditional: the model receives a partial puzzle and fills the missing cells, with clue positions pinned at every sampling step. We measure validity, the fraction of generated solutions satisfying all constraints, on 1,000 held-out partial puzzles at NFE = 128. As a discrete baseline, we use masked diffusion model (MDM) Sahoo et al. (2024), where p is the power in the mask schedule. The probability that a position is masked at corruption time t is $1 - (1 - t)^p$. We report $p = 1$ and $p = 0.5$. Because the vocabulary is small ($V = 10$), we use \mathbb{S}^{11} for the sphere paths and \mathbb{R}^{10} for the Euclidean paths so that the intrinsic dimension matches across paths.

Results. Using the PC sampler, see Table 1, improves accuracy substantially for vMF and VP. For VE there is no useful PC improvement. Masked, sampled predictor-only, trails the continuous methods at both schedule powers. We note that VP requires time dependent scaling of the epsilon used for PC steps (Appendix C.5.1).

5.2 Language Modeling (LM1B)

The One Billion Word Benchmark Chelba et al. (2013) is a dataset based on crawled news data.

Setup. We use the BERT-base-uncased tokenizer Devlin et al. (2019) ($N = 30,522$, $L = 128$). Training and evaluation follow MDLM Sahoo et al. (2024) and LangFlow Chen et al. (2026) with a DiT-style transformer backbone, 1M training steps, and GPT-2-large Radford et al. (2019) scoring over 1024 unconditional samples. We report generation perplexity (gen. PPL) and the average per-sample entropy H . Geodesic admits no closed-form Riemannian score and uses ODE only. We tested various sampling configurations, the choices and exact configurations are listed in C.5.3.

Baselines. As baselines we use autoregressive transformer (AR) Chen et al. (2026) which is sequential, Langflow Chen et al. (2026), Plaid Gulrajani & Hashimoto (2023), MDLM Sahoo et al. (2024), Duo Sahoo et al. (2025) and SEDD from Lou et al. (2024). As an additional reference point, we report the diagonal variant (configuration without flow-map distillation) of Potapchik et al. (2026) at same NFE. Note that LangFlow method uses self-conditioning. Without self-conditioning they report a gen. PPL of 154.2, here entropy and NFE are not given.

Results. Table 2 compares each method to the reference baselines and reports results across entropy floors. As on Sudoku, PC helps the vMF and VP paths most. The effect is most pronounced for vMF. We hypothesize that this is due to the noisy state and target embeddings having the same norm, so the network input encodes only directional

Method	Sampler	gen. PPL (\downarrow)	H (\uparrow)
<i>Reference baseline values from Chen et al. (2026)</i>			
AR	–	66.7	–
Plaid	–	77.3	–
LangFlow	–	92.2	4.31
MDLM	–	103.9	–
SEDD	–	115.9	–
Duo	–	97.6	–
<i>Time-conditioned</i>			
vMF	ODE	171.8	4.35
	PC $_{H \geq 4.30}$	112.7	4.30
	PC $_{H \geq 4.25}$	66.0	4.25
	PC $_{H \geq 4.20}$	52.4	4.21
	PC $_{H \geq 4.15}$	48.5	4.18
Geodesic	ODE	167.9	4.34
VP	ODE	140.4	4.34
	PC $_{H \geq 4.15}$	138.4	4.35
VE	ODE	149.7	4.35
	PC $_{H \geq 4.15}$	151.5	4.35
<i>Non-time-conditioned</i>			
vMF	ODE	205.5	4.38
	PC $_{H \geq 4.30}$	104.8	4.31
	PC $_{H \geq 4.15}$	77.2	4.28
Geodesic	ODE	215.5	4.37
VP	ODE	138.8	4.34
	PC $_{H \geq 4.30}$	109.4	4.31
	PC $_{H \geq 4.25}$	88.3	4.26
	PC $_{H \geq 4.20}$	77.0	4.20
	PC $_{H \geq 4.15}$	70.7	4.15
VE	ODE	195.2	4.40
	PC $_{H \geq 4.15}$	176.7	4.29
<i>Reference Potapchik et al. (2026)</i>			
DFM Diagonal	ODE	75.82	4.19

Table 2: LM1B comparison at NFE = 128. ODE is the predictor-only Euler sampler at $n = 128$. PC $_{H \geq h}$ is the best PC configuration with entropy at or above threshold. See Table 8 for details.

shows this across the entire entropy range. Relaxing the entropy floor, vMF (tc) descends to a gen. PPL of 48.5 at $H = 4.18$. This matches the DFM Diagonal entropy of $H = 4.19$ at substantially lower gen. PPL (75.82 for DFM). Without time conditioning, vMF still reaches 77.2 at $H = 4.28$. PC fails to improve VP results without entropy collapse under time conditioning.

Limitations and broader impact Our work shares the limitations of continuous diffusion approaches to discrete generation. The main technical specificity is that the conditional velocity and the radial CDF must be computed numerically, which requires care at high concentration and high embedding dimension to avoid underflow in the radial density. We address this with a flux-based ODE formulation and log-shifted density evaluation (Appendix C.3). We are not aware of any negative societal impact specific to this work beyond those that apply to generative modeling of discrete sequences in general. All experiments use public datasets.

6 Related Work

Adapting diffusion and flow-based generative models to discrete data is an active area of research. Existing approaches either work directly in the discrete state space or embed the data into a continuous space.

Our approach is closest in spirit to CDCD Dieleman et al. (2022). We use normalized embeddings, cross-entropy training, and an adaptive schedule. The key difference is that we keep the noisy state on \mathbb{S}^{d-1} throughout the generative process. In the following we highlight further related work.

Discrete state space. Discrete state space methods define Markov processes over the finite vocabulary. In general these models split into masked diffusion Sahoo et al. (2024); Campbell et al. (2022); Shi et al. (2025); Nie et al. (2025) and uniform diffusion Austin et al. (2023); Schiff et al. (2025); Sahoo et al. (2025), which converge to a special mask token or uniform random tokens respectively. D3PM Austin et al. (2023) designed discrete time forward processes. This was extended to continuous time based on the CTMC by Campbell et al. (2022). SEDD Lou et al. (2024) build a score entropy loss. Sahoo et al. (2024); Ou et al. (2026); Shi et al. (2025) introduce theoretical results and LLaDA Nie et al. (2025) scaled mask diffusion to 8 billion parameters. Recent work, GDDS Zekri et al. (2026) uses GPT-2 embeddings to induce semantic structure in discrete noising. Continuous noising in the learned embedding space follows a related intuition.

Continuous state space. Continuous embedding methods assign each token a vector and apply noise in the embedding space. Diffusion-LM Li et al. (2022) uses Gaussian DDPM with learned embeddings. Gulrajani & Hashimoto (2023) uses a discrete time process without normalized embeddings. Lee et al. (2026); Roos et al. (2026) use a linear interpolant to the one-hot target in the large \mathbb{R}^V space with a softmax denoiser and flow distillation for few-step language generation. LangFlow Chen et al. (2026) works in the continuous embedding space and introduces an ODE based NLL. In all of these the noisy state lives in \mathbb{R}^d or \mathbb{R}^V .

A separate line of work defines noise processes on the probability simplex or on spheres of dimension $|\mathcal{V}| - 1$. Generative Assignment Flows Boll et al. (2024) construct flows on the probability simplex by defining linear paths in logit space and mapping them to simplex-valued distributions via softmax. Dirichlet Flow Matching Stark et al. (2024) constructs paths from Dirichlet distributions on the simplex. RDLM Jo & Hwang (2025) uses the diffeomorphism between the simplex and the positive orthant of the sphere $\mathbb{S}^{|\mathcal{V}|-1}$ for language modeling and derives an NLL bound via Girsanov’s theorem. To simulate the bridge SDE, they split the sphere into a product of smaller spheres, since the bridge on high dimensional spheres is difficult. Davis et al. (2024); Cheng et al. (2025) map the simplex to the positive orthant of $\mathbb{S}^{|\mathcal{V}|-1}$ via the standard diffeomorphism and construct geodesic flows there.

Mixing discrete and continuous methods. A different line of work is the combination of discrete and continuous diffusion models for categorical data. Pynadath et al. (2025) propose CANDI, a hybrid discrete–continuous diffusion model with a structured forward noising process that combines a discrete masking process with Gaussian corruption. During reverse sampling, the model starts from a fully corrupted Gaussian state: positions selected to become clean are sampled from the model’s token distribution and then carried forward/fixes, while the remaining noisy positions continue to be updated by the continuous reverse ODE. Duo by Sahoo et al. (2025) shows that uniform-state

discrete diffusion arises as the argmax push-forward of an underlying Gaussian diffusion process. They exploit this duality to improve training and enable much faster few-step sampling via discrete consistency distillation.

Sudoku. For non-generative neural network approaches on Sudoku-Extreme, see Wang et al. (2025); Kornhardt et al. (2026); Jolicoeur-Martineau (2025).

7 Conclusion

We introduced a vMF path on \mathbb{S}^{d-1} for continuous generative modeling of discrete sequences. More generally, we showed that for radially symmetric paths on the sphere the continuity equation reduces to a one dimensional flux equation in the cosine similarity. For the vMF path, this reduction yields a linear ODE whose unique bounded solution gives a tractable conditional velocity. The Riemannian score follows directly from the vMF density, making ODE and predictor corrector sampling available solely from the posterior.

We applied this construction by embedding tokens as learned points on \mathbb{S}^{d-1} and training a posterior with a cross entropy loss. This posterior determines the marginal velocity and score as well as the terminal decoding probabilities. On Sudoku and LM1B, we compared vMF paths to geodesic and Euclidean baselines and showed the predictor-corrector scheme, especially for vMF, produces strong results. We believe the results show much promise and open several directions for future work.

Acknowledgments. GS acknowledge funding by the German Research Foundation (DFG) within the Excellence Cluster MATH+ and JC by project STE 571/17- 2 within the DFG-SPP 2298. GK acknowledges funding by the BMBF project VIScreenPRO (ID: 100715327).

References

- Michael S. Albergo, Nicholas M. Boffi, and Eric Vanden-Eijnden. Stochastic interpolants: A unifying framework for flows and diffusions, 2025. URL <https://arxiv.org/abs/2303.08797>.
- Luigi Ambrosio and Dario Trevisan. Well-posedness of Lagrangian flows and continuity equations in metric measure spaces. *Analysis and PDE*, 7(5):1179–1234, 2014.
- Jacob Austin, Daniel D. Johnson, Jonathan Ho, Daniel Tarlow, and Rianne van den Berg. Structured denoising diffusion models in discrete state-spaces, 2023. URL <https://arxiv.org/abs/2107.03006>.
- Bastian Boll, Daniel Gonzalez-Alvarado, and Christoph Schnörr. Generative modeling of discrete joint distributions by e-geodesic flow matching on assignment manifolds, 2024. URL <https://arxiv.org/abs/2402.07846>.
- Andrew Campbell, Joe Benton, Valentin De Bortoli, Tom Rainforth, George Deligiannidis, and Arnaud Doucet. A continuous time framework for discrete denoising models, 2022. URL <https://arxiv.org/abs/2205.14987>.
- Ciprian Chelba, Tomas Mikolov, Mike Schuster, Qi Ge, Thorsten Brants, and Phillip Koehn. One billion word benchmark for measuring progress in statistical language modeling. *CoRR*, abs/1312.3005, 2013. URL <http://arxiv.org/abs/1312.3005>.
- Jannis Chemseddine, Gregor Kornhardt, Richard Duong, and Gabriele Steidl. Adapting noise to data: Generative flows from 1d processes, 2026. URL <https://arxiv.org/abs/2510.12636>.
- Ricky T. Q. Chen and Yaron Lipman. Flow matching on general geometries, 2024. URL <https://arxiv.org/abs/2302.03660>.
- Yuxin Chen, Chumeng Liang, Hangke Sui, Ruihan Guo, Chaoran Cheng, Jiaxuan You, and Ge Liu. Langflow: Continuous diffusion rivals discrete in language modeling, 2026. URL <https://arxiv.org/abs/2604.11748>.
- Chaoran Cheng, Jiahao Li, Jian Peng, and Ge Liu. Categorical flow matching on statistical manifolds, 2025. URL <https://arxiv.org/abs/2405.16441>.

- Oscar Davis, Samuel Kessler, Mircea Petrache, İsmail İlkan Ceylan, Michael Bronstein, and Avishek Joey Bose. Fisher flow matching for generative modeling over discrete data, 2024. URL <https://arxiv.org/abs/2405.14664>.
- Jacob Devlin, Ming-Wei Chang, Kenton Lee, and Kristina Toutanova. Bert: Pre-training of deep bidirectional transformers for language understanding, 2019. URL <https://arxiv.org/abs/1810.04805>.
- Sander Dieleman, Laurent Sartran, Arman Roshannai, Nikolay Savinov, Yaroslav Ganin, Pierre H. Richemond, Arnaud Doucet, Robin Strudel, Chris Dyer, Conor Durkan, Curtis Hawthorne, Rémi Leblond, Will Grathwohl, and Jonas Adler. Continuous diffusion for categorical data, 2022. URL <https://arxiv.org/abs/2211.15089>.
- Richard Duong, Jannis Chemseddine, Peter K. Friz, and Gabriele Steidl. Telegrapher’s generative model via kac flows, 2026. URL <https://arxiv.org/abs/2506.20641>.
- Itai Gat, Tal Remez, Neta Shaul, Felix Kreuk, Ricky T. Q. Chen, Gabriel Synnaeve, Yossi Adi, and Yaron Lipman. Discrete flow matching, 2024. URL <https://arxiv.org/abs/2407.15595>.
- Zhengyang Geng, Mingyang Deng, Xingjian Bai, J. Zico Kolter, and Kaiming He. Mean flows for one-step generative modeling, 2025. URL <https://arxiv.org/abs/2505.13447>.
- Ishaan Gulrajani and Tatsunori B. Hashimoto. Likelihood-based diffusion language models, 2023. URL <https://arxiv.org/abs/2305.18619>.
- Peter Holderrieth, Marton Havasi, Jason Yim, Neta Shaul, Itai Gat, Tommi Jaakkola, Brian Karrer, Ricky T. Q. Chen, and Yaron Lipman. Generator matching: Generative modeling with arbitrary markov processes, 2025. URL <https://arxiv.org/abs/2410.20587>.
- Jaehyeong Jo and Sung Ju Hwang. Continuous diffusion model for language modeling, 2025. URL <https://arxiv.org/abs/2502.11564>.
- Alexia Jolicoeur-Martineau. Less is more: Recursive reasoning with tiny networks, 2025. URL <https://arxiv.org/abs/2510.04871>.
- Tero Karras, Miika Aittala, Timo Aila, and Samuli Laine. Elucidating the design space of diffusion-based generative models, 2022. URL <https://arxiv.org/abs/2206.00364>.
- Gregor Kornhardt, Jannis Chemseddine, Christian Wald, and Gabriele Steidl. Self-aware Markov models for discrete reasoning. In *ICLR 2026 Workshop on Logical Reasoning of Large Language Models*, 2026. URL <https://openreview.net/forum?id=2yVYK7QQKI>.
- Chanhyuk Lee, Jaehoon Yoo, Manan Agarwal, Sheel Shah, Jerry Huang, Aditi Raghunathan, Seunghoon Hong, Nicholas M. Boffi, and Jinwoo Kim. Flow map language models: One-step language modeling via continuous denoising, 2026. URL <https://arxiv.org/abs/2602.16813>.
- Xiang Lisa Li, John Thickstun, Ishaan Gulrajani, Percy Liang, and Tatsunori B. Hashimoto. Diffusion-lm improves controllable text generation, 2022. URL <https://arxiv.org/abs/2205.14217>.
- Yaron Lipman, Ricky T. Q. Chen, Heli Ben-Hamu, Maximilian Nickel, and Matt Le. Flow matching for generative modeling, 2023. URL <https://arxiv.org/abs/2210.02747>.
- Yaron Lipman, Marton Havasi, Peter Holderrieth, Neta Shaul, Matt Le, Brian Karrer, Ricky T. Q. Chen, David Lopez-Paz, Heli Ben-Hamu, and Itai Gat. Flow matching guide and code, 2024. URL <https://arxiv.org/abs/2412.06264>.
- Aaron Lou, Chenlin Meng, and Stefano Ermon. Discrete diffusion modeling by estimating the ratios of the data distribution, 2024. URL <https://arxiv.org/abs/2310.16834>.
- Kanti V. Mardia and Peter E. Jupp. *Directional Statistics*. Wiley Series in Probability and Statistics. Wiley, Chichester, 2000.
- Shen Nie, Fengqi Zhu, Zebin You, Xiaolu Zhang, Jingyang Ou, Jun Hu, Jun Zhou, Yankai Lin, Ji-Rong Wen, and Chongxuan Li. Large language diffusion models, 2025. URL <https://arxiv.org/abs/2502.09992>.

- Jingyang Ou, Shen Nie, Kaiwen Xue, Fengqi Zhu, Jiacheng Sun, Zhenguo Li, and Chongxuan Li. Your absorbing discrete diffusion secretly models the conditional distributions of clean data, 2026. URL <https://arxiv.org/abs/2406.03736>.
- William Peebles and Saining Xie. Scalable diffusion models with transformers, 2023. URL <https://arxiv.org/abs/2212.09748>.
- Peter Potapchik, Jason Yin, Adhi Saravanan, Peter Holderrieth, Eric Vanden-Eijnden, and Michael S. Albergo. Discrete flow maps, 2026. URL <https://arxiv.org/abs/2604.09784>.
- Patrick Pynadath, Jiaxin Shi, and Ruqi Zhang. Candi: Hybrid discrete-continuous diffusion models, 2025. URL <https://arxiv.org/abs/2510.22510>.
- Alec Radford, Jeff Wu, Rewon Child, David Luan, Dario Amodei, and Ilya Sutskever. Language models are unsupervised multitask learners. 2019.
- Daan Roos, Oscar Davis, Floor Eijkelboom, Michael Bronstein, Max Welling, İsmail İlkan Ceylan, Luca Ambrogioni, and Jan-Willem van de Meent. Categorical flow maps, 2026. URL <https://arxiv.org/abs/2602.12233>.
- Subham Sekhar Sahoo, Marianne Arriola, Yair Schiff, Aaron Gokaslan, Edgar Marroquin, Justin T Chiu, Alexander Rush, and Volodymyr Kuleshov. Simple and effective masked diffusion language models, 2024. URL <https://arxiv.org/abs/2406.07524>.
- Subham Sekhar Sahoo, Justin Deschenaux, Aaron Gokaslan, Guanghan Wang, Justin Chiu, and Volodymyr Kuleshov. The diffusion duality, 2025. URL <https://arxiv.org/abs/2506.10892>.
- Yair Schiff, Subham Sekhar Sahoo, Hao Phung, Guanghan Wang, Sam Boshar, Hugo Dalla-torre, Bernardo P. de Almeida, Alexander Rush, Thomas Pierrot, and Volodymyr Kuleshov. Simple guidance mechanisms for discrete diffusion models, 2025. URL <https://arxiv.org/abs/2412.10193>.
- Jiaxin Shi, Kehang Han, Zhe Wang, Arnaud Doucet, and Michalis K. Titsias. Simplified and generalized masked diffusion for discrete data, 2025. URL <https://arxiv.org/abs/2406.04329>.
- Yang Song, Jascha Sohl-Dickstein, Diederik P. Kingma, Abhishek Kumar, Stefano Ermon, and Ben Poole. Score-based generative modeling through stochastic differential equations, 2021. URL <https://arxiv.org/abs/2011.13456>.
- Hannes Stark, Bowen Jing, Chenyu Wang, Gabriele Corso, Bonnie Berger, Regina Barzilay, and Tommi Jaakkola. Dirichlet flow matching with applications to DNA sequence design, 2024. URL <https://arxiv.org/abs/2402.05841>.
- Cedric Villani. *Optimal Transport, Old and New*. Springer, 2008.
- Christian Wald and Gabriele Steidl. Flow matching: Markov kernels, stochastic processes and transport plans. In *Variational and Information Flows in Machine Learning and Optimal Transport*. Springer, 2025. doi: 10.1007/978-3-031-92731-7_4.
- Guan Wang, Jin Li, Yuhao Sun, Xing Chen, Changling Liu, Yue Wu, Meng Lu, Sen Song, and Yasin Abbasi Yadkori. Hierarchical reasoning model, 2025. URL <https://arxiv.org/abs/2506.21734>.
- Oussama Zekri, Théo Uscidda, Nicolas Boullé, and Anna Korba. Generalized discrete diffusion from snapshots, 2026. URL <https://arxiv.org/abs/2603.21342>.

A Proofs

Proposition 2.2. *Let $\mathbf{w} = (w^l)_{l=1}^L \in \mathcal{W}^L$ be fixed, and let $p_t^l(\cdot | w^l)$ be absolutely continuous measures on \mathcal{M} with velocities $v_t^l(\cdot | w^l)$ satisfying the conditional continuity equation (1) on \mathcal{M} for each $l = 1, \dots, L$. Then the product density on \mathcal{M}^L ,*

$$p_t(\mathbf{x} | \mathbf{w}) = \prod_{l=1}^L p_t^l(x^l | w^l), \quad \mathbf{x} = (x^1, \dots, x^L), \quad (2)$$

with the velocity field $v_t(\mathbf{x} | \mathbf{w}) := (v_t^1(x^1 | w^1), \dots, v_t^L(x^L | w^L))$ satisfies the continuity equation on \mathcal{M}^L for $t \in (0, 1)$.

Proof. Using the product rule we obtain

$$\partial_t p_t(\mathbf{x} | \mathbf{w}) = \sum_{l=1}^L \left(\prod_{j \neq l}^L p_t^j(x^j | w^j) \right) \partial_t p_t^l(x^l | w^l)$$

and further by the continuity equation for p_t^l ,

$$\partial_t p_t(\mathbf{x} | \mathbf{w}) = - \sum_{l=1}^L \left(\prod_{j \neq l}^L p_t^j(x^j | w^j) \right) \operatorname{div}_{\mathcal{M}}^L (p_t^l(x^l | w^l) v_t^l(x^l | w^l)).$$

Since the factor $\prod_{j \neq l}^L p_t^j(x^j | w^j)$ does not depend on x^l , we can pull it into the divergence operator, which acts only on the l -th variable which results in

$$\partial_t p_t(\mathbf{x} | \mathbf{w}) = - \sum_{l=1}^L \operatorname{div}_{\mathcal{M}}^l \left(\left(\prod_{j=1}^L p_t^j(x^j | w^j) \right) v_t^l(x^l | w^l) \right).$$

Recognizing that $p_t(\mathbf{x} | \mathbf{w}) = \prod_{j=1}^L p_t^j(x^j | w^j)$, this yields

$$\partial_t p_t(\mathbf{x} | \mathbf{w}) = - \sum_{l=1}^L \operatorname{div}_{\mathcal{M}} (p_t(\mathbf{x} | \mathbf{w}) v_t^l(x^l | w^l)).$$

Finally, using that the divergence on the product manifold \mathcal{M}^L is given as $\operatorname{div}_{\mathcal{M}^L}(u) := \sum_{l=1}^L \operatorname{div}_{\mathcal{M}}(u^l)$, we conclude

$$\partial_t p_t(\mathbf{x} | \mathbf{w}) = - \operatorname{div}_{\mathcal{M}^L} (p_t(\mathbf{x} | \mathbf{w}) v_t(\mathbf{x} | \mathbf{w})).$$

Theorem 3.2. *Let (p_t, v_t) , $t \in I$ be a sequence of radially symmetric pairs of densities and velocities of the form $p_t(x) = \bar{p}_t(\langle x, w \rangle)$, resp. $v_t(x) = \psi_t(\langle x, w \rangle) P_x(w)$, where $\bar{p}_t \in C^1[I \times (-1, 1)]$ and $\psi_t \in C^1(-1, 1)$ for every $t \in I$. Let f_t , $t \in I$ be the corresponding densities defined by (7). Then (p_t, v_t) , $t \in I$ satisfy the continuity equation*

$$\partial_t p_t + \operatorname{div}_{\mathbb{S}^{d-1}}(p_t v_t) = 0, \quad t \in I, x \in \mathbb{S}^{d-1} \setminus \{\pm w\} \quad (8)$$

if and only if (f_t, ψ_t) satisfy the one-dimensional flux equation

$$\partial_t f_t + \partial_s (f_t \psi_t \cdot (1 - s^2)) = 0, \quad t \in I, s \in (-1, 1). \quad (9)$$

Proof. Let $s := \langle w, x \rangle$. Using the divergence on the sphere we want to reformulate (8). With

$$u_t(x) := p_t(x) v_t(x) = g_t(s)(w - sx), \quad g_t := \bar{p}_t \psi_t,$$

we obtain

$$\nabla u_t(x) = g_t'(s) w(w - sx)^\top - g_t(s)(x I_d + x w^\top),$$

and further

$$\begin{aligned}\operatorname{tr}(\nabla u_t(x)) &= g'_t(s)(1-s^2) - g_t(s)(d+1)s, \\ x^\top \nabla u_t(x) &= -2sg_t(s).\end{aligned}$$

Thus, the continuity equation (8) can be rewritten as

$$\begin{aligned}0 &= \partial_t p_t + \operatorname{div}_{\mathbb{S}^{d-1}}(p_t v_t) = \nabla_t \bar{p}_t + \operatorname{tr}(\nabla u) - x^\top \nabla u_t x \\ &= \partial_t \bar{p}_t + g'_t(1-s^2) - g_t(d-1)s.\end{aligned}\quad (21)$$

On the other hand, the flux equation in (9) becomes

$$\begin{aligned}0 &= \partial_t f_t + \partial_s(g_t(1-s^2)^{(d-1)/2}) \\ &= \left((1-s^2)^{(d-3)/2} \partial_t \bar{p}_t + g'_t(1-s^2)^{(d-1)/2} + g_t(d-1)s(1-s^2)^{(d-3)/2} \right).\end{aligned}$$

Dividing by $(1-s^2)^{(d-3)/2}$, $s \in (-1, 1)$ yields equation (21) and we are done. \square

Lemma 3.3. *Let $f_t, t \in I$ be defined by (11). Then $\psi_t, t \in I$ solves the linear ODE*

$$(1-s^2)\psi'_t + (\kappa_t(1-s^2) - (d-1)s)\psi_t = (A_d(\kappa_t) - s)\dot{\kappa}_t, \quad s \in (-1, 1) \quad (12)$$

if and only if $(f_t, \psi_t), t \in I$ fulfill the flux equation (9).

Proof. For the vMF setting, the flux equation (9) reads as

$$\begin{aligned}0 &= \partial_t f_t + \partial_s(f_t \psi_t (1-s^2)) \\ &= (1-s^2)^{(d-3)/2} \partial_t \left(C_d(\kappa_t) \exp(\kappa_t s) \right) + C_d(\kappa_t) \partial_x \left((1-s^2)^{(d-1)/2} \psi_t(s) \exp(\kappa_t s) \right).\end{aligned}\quad (22)$$

Concerning the first summand, we obtain

$$\partial_t \left(C_d(\kappa_t) \exp(\kappa_t s) \right) = C'_d(\kappa_t) \dot{\kappa}_t \exp(\kappa_t s) + s \dot{\kappa}_t C_d(\kappa_t) \exp(\kappa_t s).$$

Noting that

$$\mathcal{I}'_{d/2-1}(\kappa_t) = \mathcal{I}_{d/2}(\kappa_t) + \frac{d/2-1}{\kappa_t} \mathcal{I}_{d/2-1}(\kappa_t), \quad (23)$$

we conclude

$$\begin{aligned}C'_d(\kappa_t) &= \frac{(\frac{d}{2}-1)\kappa_t^{d/2-2}}{(2\pi)^{d/2} \mathcal{I}_{d/2-1}(\kappa_t)} - \frac{\kappa_t^{d/2-1} \mathcal{I}'_{d/2-1}(\kappa_t)}{(2\pi)^{d/2} \mathcal{I}_{d/2-1}^2(\kappa_t)} \\ &= \frac{(\frac{d}{2}-1)}{\kappa_t} C_d(\kappa_t) - \frac{(\frac{d}{2}-1)}{\kappa_t} C_d(\kappa_t) - A_d(\kappa_t) C_d(\kappa_t) \\ &= -A_d(\kappa_t) C_d(\kappa_t)\end{aligned}$$

and consequently

$$\partial_t \left(C_d(\kappa_t) \exp(\kappa_t s) \right) = C_d(\kappa_t) \exp(\kappa_t s) \dot{\kappa}_t (-A_d(\kappa_t) + s). \quad (24)$$

The second summand can be rewritten as

$$\begin{aligned}\partial_s \left((1-s^2)^{(d-1)/2} \psi_t(s) \exp(\kappa_t s) \right) &= -(d-1)(1-s^2)^{(d-3)/2} x \psi_t(s) \exp(\kappa_t s) \\ &+ (1-s^2)^{(d-1)/2} \psi'_t(s) \exp(\kappa_t s) + \kappa_t (1-s^2)^{(d-1)/2} \psi_t(s) \exp(\kappa_t s)\end{aligned}\quad (25)$$

Plugging in (24) and (25) into (22) and dividing by $C_d(\kappa_t)(1-s^2)^{(d-3)/2} \exp(\kappa_t s)$ yields

$$\dot{\kappa}_t (A_d(\kappa_t) - s) = (-(d-1)s + (1-s^2)\kappa_t) \psi_t(s) + (1-s^2) \psi'_t(s).$$

This finishes the proof. \square

Lemma 3.4. *For any $t \in I$, the ODE (12) has a unique solution ψ_t in $C[-1, 1]$, which is automatically also in $C^\infty(-1, 1)$ with boundary values $\psi_t(1) = \frac{(1-A_d(\kappa_t))\dot{\kappa}_t}{d-1}$, and $\psi_t(-1) = \frac{(1+A_d(\kappa_t))\dot{\kappa}_t}{d-1}$.*

Proof. The general solution of the linear ODE

$$\psi' + \left(\kappa - (d-1) \frac{s}{1-s^2} \right) \psi = (A_d - s) \frac{\dot{\kappa}}{1-s^2}, \quad s \in (-1, 1)$$

(with skipped index t for convenience) can be computed by the method of integrating factors as

$$\psi(s) = \exp(-\kappa s)(1-s^2)^{-(d-1)/2} \left(C + \dot{\kappa} \int_{-1}^s \exp(\kappa y)(1-y^2)^{(d-3)/2} (A_d - y) dy \right),$$

where the constant C is determined by conditions on ψ . We are interested in solutions with finite $\lim_{s \rightarrow \pm 1} \psi(s)$. Since $(1-s^2)^{-(d-1)/2}$ goes to infinity as $s \rightarrow \pm 1$, this can only be achieved for $C = 0$ and the solution

$$\psi(s) = \dot{\kappa} \exp(-\kappa s)(1-s^2)^{-(d-1)/2} \int_{-1}^s \exp(\kappa y)(1-y^2)^{(d-3)/2} (A_d - y) dy. \quad (26)$$

Indeed the integral behaves for s near -1 as $(s+1)^{(d-1)/2}$, so that $\psi(-1)$ is finite and the concrete value follows immediately from (12). On the other hand, considering $s \rightarrow 1$, we have

$$\int_{-1}^1 \exp(\kappa y)(1-y^2)^{(d-3)/2} (A_d - y) dy = A_d G(\kappa) - G'(\kappa)$$

where

$$G(\kappa) := \int_{-1}^1 \exp(\kappa y)(1-y^2)^{(d-3)/2} dy = \mathcal{I}_{d/2-1}(\kappa) \alpha(\kappa), \quad \alpha(\kappa) := \frac{\Gamma((d-1)/2) \sqrt{\pi}}{(\kappa/2)^{(d/2-1)}}$$

and using (23) and the definition of A_d further

$$A_d G(\kappa) - G'(\kappa) = \mathcal{I}_{d/2}(\kappa) \alpha(\kappa) - \left(\mathcal{I}_{d/2}(\kappa) + \frac{d/2-1}{\kappa} \mathcal{I}_{d/2-1}(\kappa) \right) \alpha(\kappa) - \mathcal{I}_{d/2-1}(\kappa) \alpha'(\kappa) = 0.$$

The asymptotics of the integral in (26) as $s \rightarrow 1$ is $(s-1)^{(d-1)/2}$. Finally, the representation (26) is a product of functions that are smooth on $(-1, 1)$, so that $\psi \in C^\infty(-1, 1)$ and we are done. \square

Theorem 3.5. *Let $p_t(\cdot|w)$ be the conditional vMF path defined by (10) and let $\psi_t, t \in I$ be the unique $C[-1, 1]$ solutions of the ODE (12). Then $p_t(\cdot|w)$ together with the velocities*

$$v_t(x|w) = \psi_t(\langle w, x \rangle) P_x(w)$$

fulfill the continuity equation (8) on \mathbb{S}^{d-1} .

Proof. By the previous proofs we have for the corresponding expressions in (9), (12) and (8) that

$$\begin{aligned} (14) &= C_d(\kappa_t)(1-s^2)^{(d-3)/2} \exp(\kappa_t s) \cdot (18) \\ &= (1-s^2)^{(d-3)/2} \cdot (13), \end{aligned}$$

where (13) = $R(s) = \partial_t \bar{p}_t(s) + g'_t(s)(1-s^2) - g_t(s)(d-1)s$ and $g_t(s) = C_d(\kappa_t) \exp(\kappa_t s) \psi_t(s)$. This gives the assertion for $s \in (-1, 1)$. For the chosen ψ , we have that R is continuous on $[-1, 1]$ (note that $\psi'_t(\pm 1)$ is also finite) and since R is zero on $(-1, 1)$ by (12), it remains zero at the boundary. So we have an extension of the relation to the whole \mathbb{S}^{d-1} . \square

Proposition 3.7. *Let $X_0 \sim \mathcal{U}(\mathbb{S}^{d-1})$ and $w \in \mathbb{S}^{d-1}$ be arbitrary fixed. Then the conditional geodesic interpolation path (slerp) in (6) fulfill*

$$\mathbb{E}_{x_t \sim \text{slerp}_{p_t}(x_0, w)}[\langle w, x_t \rangle] \rightarrow \sin\left(\frac{\pi}{2} t\right) \quad \text{as } d \rightarrow \infty, \quad (14)$$

the vMF path (10),

$$\mathbb{E}_{x_t \sim \text{vMF}(w, \kappa_t)}[\langle w, x_t \rangle] = A_d(\kappa_t) = \frac{\kappa_t}{d} + O(\kappa_t^3). \quad (15)$$

Proof. Since (15) was already stated, it remains to verify (14). For

$$X_t = \frac{\sin((1-t)\theta)}{\sin\theta} X_0 + \frac{\sin(t\theta)}{\sin\theta} w,$$

let $Z_t := \langle w, X_t \rangle$. By Remark 3.1, we know that

$$Z_t = \cos((1-t)\Theta), \quad \Theta = \arccos(\langle w, X_0 \rangle).$$

It is straightforward to check that Z_0 is a random variable on $[-1, 1]$ with expectation value zero and variance $1/d$. Thus, $Z_0 \rightarrow 0$ as $d \rightarrow \infty$ in probability and consequently $\Theta \rightarrow \pi/2$ in probability as $d \rightarrow \infty$, and finally

$$Z_t \rightarrow \cos\left((1-t)\frac{\pi}{2}\right) \quad \text{as } d \rightarrow \infty$$

in probability. Then the bounded convergence theorem gives

$$\mathbb{E}[Z_t] \rightarrow \cos\left((1-t)\frac{\pi}{2}\right) = \sin\left(\frac{\pi}{2}t\right) \quad \text{as } d \rightarrow \infty. \quad \square$$

Proposition 4.1. *The minimizer of (17) is the per-position marginal posterior $p_t^l(\cdot|\mathbf{x})$ from (4).*

Proof. We show that the loss (17) decomposes as

$$\mathcal{L}(\theta) = \sum_{l=1}^L \mathbb{E}_{t \sim \mathcal{U}(0,1), \mathbf{x}_t \sim p_t} \left[\text{CE}(p_t^l(\cdot|\mathbf{x}_t), p_{\theta,t}^l(\cdot|\mathbf{x}_t)) \right], \quad (27)$$

from which the claim follows by the minimization property above. Write $\mathcal{L} = \sum_{l=1}^L \mathcal{L}^l$, where

$$\mathcal{L}^l(\theta) := - \int \int \sum_{\mathbf{w} \in \mathcal{W}^L} \log p_{\theta,t}^l(w^l|\hat{x}_t^l) p_t(\mathbf{x}_t|\mathbf{w}) p_{\text{data}}(\mathbf{w}) d\mathbf{x}_t dt.$$

By Bayes' rule and since $\log p_{\theta,t}^l(w^l|\hat{x}_t^l)$ depends on \mathbf{w} only through w^l , this can be rewritten as

$$\begin{aligned} \mathcal{L}^l(\theta) &= - \int \int \sum_{\mathbf{w} \in \mathcal{W}^L} \log p_{\theta,t}^l(w^l|\hat{x}_t^l) p_t(\mathbf{w}|\mathbf{x}_t) p_t(\mathbf{x}_t) d\mathbf{x}_t dt \\ &= - \int \int \sum_{w^l \in \mathcal{W}} \log p_{\theta,t}^l(w^l|\hat{x}_t^l) \sum_{\substack{w^j \in \mathcal{W} \\ j \neq l}} p_t(\mathbf{w}|\mathbf{x}_t) p_t(\mathbf{x}_t) d\mathbf{x}_t dt \\ &= \mathbb{E}_{t, \mathbf{x}_t \sim p_t} \left[\text{CE}(p_t^l(\cdot|\mathbf{x}_t), p_{\theta,t}^l(\cdot|\hat{x}_t^l)) \right], \end{aligned}$$

which is (27). □

B SDE Sampling on the Sphere

B.1 Fokker–Planck and the flow SDE

The same flow of measures from Section 2 admits a stochastic realization once the score is available. Substituting $v_t = u_t - \frac{\sigma^2}{2} \nabla_{\mathcal{M}} \log p_t$ for $\sigma > 0$ and using $\text{div}_{\mathcal{M}}(\nabla_{\mathcal{M}} g) = \Delta_{\mathcal{M}} g$, the continuity equation (CE) becomes the *Fokker–Planck equation*

$$\partial_t p_t + \text{div}_{\mathcal{M}}(p_t u_t) - \frac{\sigma^2}{2} \Delta_{\mathcal{M}} p_t = 0.$$

The solution p_t is the law of a random variable X_t determined by the *flow SDE*

$$dX_t = u_t(X_t) dt + \sigma dB_t, \quad (\text{Flow SDE})$$

where B_t is the Brownian motion on \mathcal{M} . Once v_t and $\nabla_{\mathcal{M}} \log p_t$ are known, sampling from p_t can be done either deterministically via the flow ODE (Flow ODE) or stochastically via the SDE (Flow SDE).

B.2 Marginal SDE for the vMF path

The score (19) enables stochastic sampling along the same marginal path. The flow SDE on $(\mathbb{S}^{d-1})^L$ reads per position

$$dX_t^l = \left[v_t^l(\mathbf{X}_t) + \frac{\sigma^2}{2} \nabla_{\mathbb{S}^{d-1}, x^l} \log p_t(\mathbf{X}_t) \right] dt + \sigma dB_t^l, \quad l = 1, \dots, L, \quad (28)$$

where $\sigma > 0$ is a free diffusion coefficient and B_t^l is Brownian motion on \mathbb{S}^{d-1} . Substituting (18) and (19), the drift of (28) is itself a posterior-weighted tangent sum,

$$v_t^l + \frac{\sigma^2}{2} \nabla_{\mathbb{S}^{d-1}, x^l} \log p_t = \sum_{k=1}^N p_t^l(w_k | \mathbf{x}) \left(\dot{\kappa}_t \tilde{\psi}_t(\langle w_k, x^l \rangle) + \frac{\sigma^2}{2} \kappa_t \right) P_{x^l}(w_k), \quad (29)$$

with the same posteriors and tangent projections as the ODE. No separate score network is required. Algorithm 1 discretizes (28) via Euler–Maruyama with a tangent retraction.

Algorithm 1 SDE sampling on $(\mathbb{S}^{d-1})^L$

Require: Time grid $0 = t_0 < t_1 < \dots < t_S = 1$, diffusion coefficient $\sigma > 0$

- 1: Sample $x_0^l \sim \mathcal{U}(\mathbb{S}^{d-1})$ independently for $l = 1, \dots, L$
 - 2: **for** $n = 0, \dots, S - 1$ **do**
 - 3: $\Delta t \leftarrow t_{n+1} - t_n$
 - 4: $(\hat{x}^1, \dots, \hat{x}^L) \leftarrow T_\theta(x_n^1, \dots, x_n^L)$
 - 5: $p_k^l \leftarrow p_\theta^l(w_k | \hat{x}^l)$ for all l, k
 - 6: $d^l \leftarrow \sum_{k=1}^N p_k^l \left(\dot{\kappa}_{t_n} \tilde{\psi}_{t_n}(\langle w_k, x_n^l \rangle) + \frac{\sigma^2}{2} \kappa_{t_n} \right) P_{x_n^l}(w_k)$ ▷ (29)
 - 7: Sample $\xi^l \sim \mathcal{N}(0, I_d)$ for $l = 1, \dots, L$
 - 8: $x_{n+1}^l \leftarrow \frac{x_n^l + \Delta t d^l + \sigma \sqrt{\Delta t} P_{x_n^l}(\xi^l)}{\|x_n^l + \Delta t d^l + \sigma \sqrt{\Delta t} P_{x_n^l}(\xi^l)\|}$ for $l = 1, \dots, L$
 - 9: **end for**
 - 10: $(\hat{x}^1, \dots, \hat{x}^L) \leftarrow T_\theta(x_S^1, \dots, x_S^L)$
 - 11: **return** $\hat{y}^l = \arg \max_{k=1, \dots, N} \langle w_k, \hat{x}^l \rangle + b_k$ for $l = 1, \dots, L$
-

C Implementation Details

C.1 Architecture and training

All continuous methods share a DiT-style transformer backbone with adaLN conditioning. When time conditioning is off, adaLN reduces to a learnable per-block scale, shift, and gate. Otherwise it receives the schedule parameter normalized to $[0, 1]$. Embeddings are tied to the softmax classifier head as described in Section 4. We use AdamW with mixed-precision (bf16) training, a linear warmup followed by a cosine learning-rate schedule, and an exponential moving average on the network weights, which is the version used at sampling time. Masked diffusion uses the same backbone but with a discrete embedding layer of width equal to the hidden size, replacing the tied learned embeddings on the manifold. Per-task hyperparameters are listed in Table 3.

C.2 Compute Resources

For the Sudoku experiments, we use an NVIDIA RTX 6000 Ada, and for LM1B we use $2 \times$ NVIDIA H200 for approximately 2 days.

C.3 Conditional paths

vMF path. Embeddings are constrained to the unit sphere by normalization. The terminal concentration κ_{\max} is set per task. We use $\kappa_{\max} = 15$ for Sudoku and $\kappa_{\max} = 250$ for LM1B. We precompute two 2D tables on a uniform grid $(\mu_i, \kappa_j) \in [-1, 1] \times [0, \kappa_{\max}]$, one for the velocity

	Sudoku	LM1B
Hidden size	512	768
Blocks	8	12
Parameters	28.6M	116.4M
Sequence length L	81	128
Vocabulary N	10	30,522
Training steps	1,000,000	1,000,000
Batch size	128	128 per GPU, eff. 512
Learning rate	3×10^{-4}	3×10^{-4}
Warmup steps	1,000	2,500
EMA decay	0.999	0.9999
Dropout	0.1	0.1
Gradient clip	1.0	1.0
Precision	bf16	bf16

Table 3: Architecture and training hyperparameters per task.

scalar $\tilde{\psi}(\mu, \kappa)$ and one for the radial CDF used in sampling. Both are queried at runtime by bilinear interpolation, so the per-step cost of a vMF velocity evaluation matches that of a Euclidean path up to the $L \times N$ posterior sum that all paths share.

Velocity lookup. The function $\tilde{\psi}(\mu, \kappa)$ in (13) is schedule-independent and depends only on the cosine similarity $\mu = \langle w, x \rangle$ and the concentration κ . The flux representation

$$\tilde{\psi}(\mu, \kappa) = -\frac{\int_{-1}^{\mu} (y - A_d(\kappa)) f(y; \kappa) dy}{f(\mu; \kappa) (1 - \mu^2)}$$

is evaluated by a cumulative trapezoid sum along the μ -axis. The unnormalized radial density $f(\mu; \kappa) = (1 - \mu^2)^{(d-3)/2} \exp(\kappa\mu)$ varies over many orders of magnitude for large d or κ . We avoid underflow by working with $g(\mu) = \exp(\log f(\mu) - \max_{\mu} \log f)$, where the shift cancels in the ratio. Near $\mu \rightarrow \pm 1$ where g underflows, the analytical boundary values from Lemma 3.3 are blended smoothly with the interior solution. The Bessel ratio $A_d(\kappa) = \mathcal{I}_{d/2}(\kappa) / \mathcal{I}_{d/2-1}(\kappa)$ is evaluated by a backward continued fraction.

Training-time sampling. Each position requires a sample $x^l \sim \text{vMF}(w^l, \kappa_t)$. By radial symmetry, every sample decomposes as $x = \mu w + \sqrt{1 - \mu^2} v$, where v is a random unit vector in the tangent plane at w . The tangent component v is obtained by projecting a standard Gaussian onto the tangent plane and normalising. The cosine μ is sampled by inverse CDF: we precompute the CDF of $f(\mu; \kappa)$ on the same 2D grid via cumulative integration, draw $u \sim \mathcal{U}(0, 1)$, and invert by interpolation at runtime.

Geodesic path. Embeddings are constrained to the unit sphere. The conditional path is the SLERP interpolant of Remark 3.1 between a uniformly sampled point and the target embedding, indexed by $t \in [0, 1]$. There is no closed-form Riemannian score for this path, so the predictor-corrector sampler is unavailable.

VP path. Embeddings are unconstrained vectors in \mathbb{R}^d . The conditional path is $h_t = (1 - t)Z + tw$ with $Z \sim \mathcal{N}(0, I_d)$, indexed by $t \in [0, 1]$. The marginal score (5) diverges as $t \rightarrow 1$. At inference we cap the predictor and corrector below $t = 1 - 10^{-3}$ to avoid division by zero.

VE path. Following Dieleman et al. (2022) embeddings are vectors in \mathbb{R}^d rescaled to norm \sqrt{d} so that the per-coordinate variance of clean embeddings matches the additive Gaussian noise. The conditional path is $h_t = w + \sigma_t Z$ with $Z \sim \mathcal{N}(0, I_d)$ and $\sigma_t \in [0, \sigma_{\max}]$. We use $\sigma_{\max} = 300$ for both Sudoku and LM1B. Following Karras et al. (2022); Dieleman et al. (2022), we apply input preconditioning, the network sees $h_t / \sqrt{\sigma_t^2 + 1}$ rather than h_t directly. Combined with the \sqrt{d} embedding scale, this gives the network input a per-coordinate variance independent of σ_t . The marginal score diverges as $\sigma_t \rightarrow 0$, so at inference we floor σ_t at 10^{-3} .

Masked diffusion baseline. Tokens are corrupted by an absorbing-state continuous-time Markov chain at rate $t \in [0, 1]$, following Sahoo et al. (2024). The model predicts the clean token from a partially masked sequence and is trained with a cross-entropy loss restricted to masked positions. The mask schedule is fixed (not learned) as $m(t) = 1 - (1 - t)^p$ for a power $p > 0$, where $m(t)$ is the probability that a position is masked at corruption time t . Thus p controls the curvature of the corruption schedule: $p = 1$ is linear, $p < 1$ masks fewer positions at intermediate times, and $p > 1$ masks more positions at intermediate times. On Sudoku we report $p = 1$ and $p = 0.5$. The optimal posterior is time-independent Gat et al. (2024), so we do not condition the backbone on time for the masked baseline.

C.4 Adaptive schedule

We give details of the adaptive schedule introduced in Remark 4.2. The loss (17) expects $t \sim \mathcal{U}(0, 1)$. In practice we sample t from a learned distribution F on $[0, 1]$ that concentrates mass where the per-sample cross-entropy varies fastest along t . The same scheme is used for every conditional path.

Parametrization. The warp $\tilde{F} : [0, 1] \rightarrow \mathbb{R}_{\geq 0}$ is piecewise linear with N bins, parametrized by two sets of logits $\ell^{(\text{in})}, \ell^{(\text{out})} \in \mathbb{R}^N$, both initialized to $-\log N$ so that the warp starts as the identity. Input bin widths are $\text{softmax}(\ell^{(\text{in})})$. Output heights come from $\text{softmax}(\ell^{(\text{out})})$ for the normalized CDF F and from $\exp(\ell^{(\text{out})})$ for the unnormalized \tilde{F} . Values $\tilde{F}(t)$ and $F(t)$ are obtained by linear interpolation within the bin containing t .

Fitting. Let

$$\ell(\mathbf{w}, \mathbf{x}_t) = -\frac{1}{L} \sum_{l=1}^L \log p_{\theta, t}^l(w^l | \hat{x}_t^l)$$

be the per-sample cross-entropy at the current t . We fit \tilde{F} by minimizing

$$\mathcal{L}_{\text{warp}} = \mathbb{E}_t \left[(F(t) \cdot \tilde{F}(1) - \ell(\mathbf{w}, \mathbf{x}_t))^2 \right],$$

with $F = \tilde{F} / \tilde{F}(1)$, so that F approximates the cumulative loss curve normalized to $[0, 1]$. A more flexible variant raises F to a power $\beta > 0$ before regression, which sharpens or flattens the resulting CDF. We use the linear case throughout.

Sampling. Given the fitted F , we draw t by inverse-transform sampling: $u \sim \mathcal{U}(0, 1)$ and $t = F^{-1}(u)$. Inversion is exact and amounts to evaluating the same piecewise-linear interpolator with input and output edge sequences swapped.

C.5 Inference ablation

This section documents the predictor-corrector sweep underlying Tables 1 and 2. Section C.5.1 defines the three sweep axes and notation. Section C.5.2 reports the per-method grids and best configurations for Sudoku. Section C.5.3 reports the same for LM1B.

C.5.1 Sweep choices

The predictor-corrector sampler of Algorithm 2 has three components that we sweep uniformly across all paths admitting a closed-form score.

NFE split. Each predictor step is followed by k Langevin corrector steps, so $\text{NFE} = n(1 + k)$. At fixed $\text{NFE} = 128$ we sweep $(n, k) \in \{(64, 1), (32, 3), (16, 7)\}$.

Predictor spacing. By default the n predictor steps are placed uniformly in training time t . The warp-aware variant places them uniformly in the warp coordinate $F(t) \in [0, 1]$ instead, so that steps concentrate where the loss curve is steepest. The flag `w` marks warp-aware spacing, its absence marks uniform spacing.

Corrector step size. The corrector uses step size ε on a per-task grid (Sections C.5.2 and C.5.3). With damping the effective step size is $\varepsilon_{\text{eff}} = \varepsilon(1 - u)^2$, where $u \in [0, 1]$ is a path-specific progress variable running from 0 at the noise end to 1 at the clean end. We set $u = \kappa_t/\kappa_{\text{max}}$ for vMF, $u = t$ for VP, and $u = 1 - \sigma_t/\sigma_{\text{max}}$ for VE, so that the arrow of progress is unified across paths. Damping suppresses Langevin correction near the clean end, where Euclidean scores can be singular. Empirically, damping is required for VP and VE to PC-sample at all. Without it, the corrector collapses across the entire ε grid (Appendix C.5.2). On vMF the two formulas are within roughly one point of each other, consistent with the score being bounded uniformly in the state. The flag `d` marks damping on, its absence marks damping off.

A configuration is specified by a tuple $((n, k), \varepsilon, \text{flags})$, where `flags` $\in \{\text{w}, \text{d}, \text{wd}, -\}$ encodes the two choices. Here `w` stands for warp-aware spacing alone, `d` for damping alone, `wd` for both, and `-` for neither. Geodesic and masked diffusion are sampled with the predictor only.

Algorithm 2 ODE / predictor-corrector sampling on $(\mathbb{S}^{d-1})^L$

Require: Time grid $0 = t_0 < t_1 < \dots < t_n = 1$, corrector steps $k \geq 0$, step size $\varepsilon > 0$

- 1: Sample $x_0^l \sim \mathcal{U}(\mathbb{S}^{d-1})$ independently for $l = 1, \dots, L$
- 2: **for** $i = 0, \dots, n - 1$ **do**
- 3: $(\hat{x}^1, \dots, \hat{x}^L) \leftarrow T_\theta(x_i^1, \dots, x_i^L)$
- 4: $p_j^l \leftarrow p_\theta^l(w_j \mid \hat{x}^l)$ for all l, j
- 5: $v^l \leftarrow \dot{\kappa}_{t_i} \sum_{j=1}^N p_j^l \tilde{\psi}_{t_i}(\langle w_j, x_i^l \rangle) P_{x_i^l}(w_j)$ for $l = 1, \dots, L$ ▷ (18)
- 6: $x_{i+1}^l \leftarrow \frac{x_i^l + (t_{i+1} - t_i) v^l}{\|x_i^l + (t_{i+1} - t_i) v^l\|}$ for $l = 1, \dots, L$
- 7: **for** $j = 1, \dots, k$ **do** ▷ Langevin corrector
- 8: $(\hat{x}^1, \dots, \hat{x}^L) \leftarrow T_\theta(x_{i+1}^1, \dots, x_{i+1}^L)$ ▷ fresh forward at corrected state
- 9: $p_m^l \leftarrow p_\theta^l(w_m \mid \hat{x}^l)$ for all l, m
- 10: Sample $\xi^l \sim \mathcal{N}(0, I_d)$ for $l = 1, \dots, L$
- 11: $g^l \leftarrow \kappa_{t_{i+1}} \sum_{m=1}^N p_m^l P_{x_{i+1}^l}(w_m)$ for $l = 1, \dots, L$ ▷ score, (19)
- 12: $\eta^l \leftarrow P_{x_{i+1}^l}(\varepsilon g^l + \sqrt{2\varepsilon} \xi^l)$ for $l = 1, \dots, L$ ▷ project to tangent
- 13: $x_{i+1}^l \leftarrow \frac{x_{i+1}^l + \eta^l}{\|x_{i+1}^l + \eta^l\|}$ for $l = 1, \dots, L$ ▷ retract to sphere
- 14: **end for**
- 15: **end for**
- 16: $(\hat{x}^1, \dots, \hat{x}^L) \leftarrow T_\theta(x_n^1, \dots, x_n^L)$
- 17: **return** $\hat{y}^l = \arg \max_{j=1, \dots, N} \langle w_j, \hat{x}^l \rangle + b_j$ for $l = 1, \dots, L$ ▷ (20)

C.5.2 Sudoku sweep

We report two views of the sweep here: the per-method validity grids in Tables 5, 6, and 7, and the configuration achieving each PC entry of Table 1 in Table 4.

The PC sweep on Sudoku uses the per-task corrector step size $\varepsilon \in \{10^{-3}, 10^{-2}, 10^{-1}, 1, 2\}$ at NFE = 128, with $\varepsilon = 2$ included as a saturation check. Tables 5–7 report the validity at each $((n, k), \varepsilon)$, taking the best across the warp and damping flags per cell. Table 4 lists the configuration achieving each PC entry of Table 1.

Method	Validity	Configuration
<i>Time-conditioned</i>		
vMF	0.747	(32, 3), $\varepsilon = 1$, d
VP	0.678	(16, 7), $\varepsilon = 1$, d
VE	0.506	(16, 7), $\varepsilon = 10^{-3}$, wd
<i>Non-time-conditioned</i>		
vMF	0.792	(64, 1), $\varepsilon = 1$, wd
VP	0.736	(64, 1), $\varepsilon = 1$, d
VE	0.544	(16, 7), $\varepsilon = 10^{-3}$, d

Table 4: Configurations behind the PC entries of Table 1.

$(n, k) \setminus \varepsilon$	10^{-3}	10^{-2}	10^{-1}	1
<i>Time-conditioned</i>				
(64, 1)	0.681	0.712	0.741	0.735
(32, 3)	0.693	0.730	0.745	0.747
(16, 7)	0.688	0.732	0.737	0.658
<i>Non-time-conditioned</i>				
(64, 1)	0.583	0.650	0.755	0.792
(32, 3)	0.589	0.650	0.689	0.668
(16, 7)	0.593	0.660	0.668	0.570

Table 5: Sudoku PC grid for vMF. ODE baselines: tc 0.658 (uniform) / 0.626 (warp-aware). Non-tc 0.564 (uniform) / 0.556 (warp-aware).

$(n, k) \setminus \varepsilon$	10^{-3}	10^{-2}	10^{-1}	1
<i>Time-conditioned</i>				
(64, 1)	0.531	0.543	0.601	0.658
(32, 3)	0.528	0.546	0.616	0.668
(16, 7)	0.529	0.547	0.633	0.678
<i>Non-time-conditioned</i>				
(64, 1)	0.542	0.560	0.610	0.736
(32, 3)	0.543	0.561	0.637	0.731
(16, 7)	0.551	0.562	0.645	0.733

Table 6: Sudoku PC grid for VP. ODE baselines: tc 0.534 (uniform) / 0.526 (warp-aware). Non-tc 0.548 (uniform) / 0.531 (warp-aware).

$(n, k) \setminus \varepsilon$	10^{-3}	10^{-2}	10^{-1}	1
<i>Time-conditioned</i>				
(64, 1)	0.484	0.419	0.375	0.422
(32, 3)	0.495	0.277	0.059	0.022
(16, 7)	0.506	0.002	0.078	0.000
<i>Non-time-conditioned</i>				
(64, 1)	0.528	0.499	0.471	0.490
(32, 3)	0.536	0.336	0.018	0.019
(16, 7)	0.544	0.007	0.028	0.000

Table 7: Sudoku PC grid for VE. ODE baselines: tc 0.464 (uniform) / 0.480 (warp-aware). Non-tc 0.518 (uniform) / 0.534 (warp-aware).

C.5.3 LM1B sweep

The PC sweep on LM1B uses the per-task corrector step size $\varepsilon \in \{10^{-5}, \dots, 10^{-1}\}$. Table 8 lists, for every (method, sampler, entropy floor) cell of Table 2, the configuration that achieves the lowest PPL among all PC configurations satisfying the floor. Methods that plateau under PC are reported as a single PC row at the lowest reachable floor. Methods that descend continuously have one row per floor.

Document-separator alignment with reference dataloaders. Our data preparation script uses [SEP] (id 102) as the document separator, while the reference dataloaders of Sahoo et al. (2024); Chen et al. (2026) derive the marker via `tokenizer.encode()[0]` and use [CLS] (id 101). The two tokens re-tokenize to different GPT-2 BPE sequences and would otherwise bias the perplexity comparison. We remap $102 \rightarrow 101$ at decode time before scoring.

C.6 LM1B qualitative samples

Each block shows the first decoded sequence from a selected row.

vMF
<p>ODE, warp-aware, $n = 128$ PPL = 205.52, $H = 4.375$.</p>

Method	Sampler	PPL (\downarrow)	H	Configuration
<i>Time-conditioned</i>				
vMF	ODE	171.8	4.35	warp-aware, $n = 128$
	PC, $H \geq 4.30$	112.7	4.30	$(64, 1)$, $\varepsilon = 10^{-3}$, wd
	PC, $H \geq 4.25$	66.0	4.25	$(32, 3)$, $\varepsilon = 10^{-3}$, -
	PC, $H \geq 4.20$	52.4	4.21	$(32, 3)$, $\varepsilon = 10^{-3}$, w
VP	PC, $H \geq 4.15$	48.5	4.18	$(16, 7)$, $\varepsilon = 10^{-3}$, w
	ODE	140.4	4.34	warp-aware, $n = 128$
VE	PC, $H \geq 4.15$	138.4	4.35	$(64, 1)$, $\varepsilon = 10^{-2}$, wd
	ODE	149.7	4.35	warp-aware, $n = 128$
Geodesic	PC, $H \geq 4.15$	151.5	4.35	$(64, 1)$, $\varepsilon = 10^{-5}$, wd
	ODE	167.9	4.34	warp-aware, $n = 128$
<i>Non-time-conditioned</i>				
vMF	ODE	205.5	4.38	warp-aware, $n = 128$
	PC, $H \geq 4.30$	104.8	4.31	$(16, 7)$, $\varepsilon = 10^{-2}$, d
	PC, $H \geq 4.15$	77.2	4.28	$(16, 7)$, $\varepsilon = 10^{-2}$, wd
VP	ODE	138.8	4.34	warp-aware, $n = 128$
	PC, $H \geq 4.30$	109.4	4.31	$(64, 1)$, $\varepsilon = 10^{-1}$, wd
	PC, $H \geq 4.25$	88.3	4.26	$(64, 1)$, $\varepsilon = 0.3$, wd
	PC, $H \geq 4.20$	77.0	4.20	$(32, 3)$, $\varepsilon = 0.3$, wd
	PC, $H \geq 4.15$	70.7	4.15	$(16, 7)$, $\varepsilon = 0.3$, wd
VE	ODE	195.2	4.40	warp-aware, $n = 128$
	PC, $H \geq 4.30$	190.3	4.37	$(32, 3)$, $\varepsilon = 10^{-5}$, d
	PC, $H \geq 4.15$	176.7	4.29	$(16, 7)$, $\varepsilon = 10^{-3}$, d
Geodesic	ODE	215.5	4.37	warp-aware, $n = 128$

Table 8: Configurations behind every (method, sampler, entropy floor) cell of Table 2.

[CLS]k up 28 % favorubius. [CLS] bank of america, which raised about 100 employees by june 2008, has had no intention of failing to reform into votes, unlike others. [CLS] rumlairer believed the u. s. reported 30 dead at the scene, but he ' s not known yet has decided to distance him to neutralize the assaults to the two pakistanis since their father had moved on operations. [CLS] it is notable that the sony can be too close to its original birthday right itself, " the source said. [CLS] its plans include selling apartments in west israel, now on the premises of most of its stores in [CLS]

PC, $(16, 7)$, $\varepsilon = 10^{-2}$, d
PPL = 104.79, $H = 4.310$.

[CLS] with the exterior it feels like a seat store. [CLS] they want to make a real game like they ' re cutting the box. [CLS] the move also pushed the electronic manufacturer more firmly in the hands of most of the market for monday, while propair has a joint venture with channel design, the consumer chemical group. [CLS] others, too, said they were optimistic about the switch to last at least a month. [CLS] the european union says it needs to regain its stance immediately after the polls. [CLS] " i was a glamorous mom and a great citizen, " mr. joonus said in 2001 in the trial of two people [CLS]

PC, $(16, 7)$, $\varepsilon = 10^{-2}$, wd
PPL = 77.19, $H = 4.276$.

[CLS] ll be able to connect alongside these wind steps! [CLS] " not to see people understand anything that i ' m going to do. [CLS] the bulldogs fell to within 24 - 19 late in the second half. [CLS] the agency needed an alternate place to get the balance on the contact lists. [CLS] and at a time when the recording world is finally dipping the head in the fabric, it ' s continuing to stress. [CLS] the other automatic formula is expected to be completed by the end of november. [CLS] it was unusual for those in mogadishu to push the president, former leader omari abe, to the airport in the city [CLS]

vMF, time-conditioned

ODE, warp-aware, $n = 128$
PPL = 171.78, $H = 4.350$.

[CLS] my savings to save her south the school rooms, " he said. [CLS] rajabaradei said there are two successful long - term measures to help deliver poverty, requiring a potent increase in economic markets that thus rarely smooth for impoverished poor people who commit itself back to waste by year ' s record doublet crude dip. [CLS] cartwright was appointed a named sales chairman by director julie lynn, 40, on " entourage, " which came out into line by the end of the month, going a mile after his £40 tires was paid from its general secretary - general party. [CLS] a more information about stclo is relaunched. [CLS] [CLS]

PC, (64, 1), $\varepsilon = 10^{-3}$, wd
PPL = 112.73, $H = 4.300$.

[CLS] fasting 13 points on purdue ' s next 27 possessions, or south carolina beat houston, 44 - 77. [CLS] harry tom hammond, the son of sir harry o ' brien, has pulled off a free letter from derby city london, which is also the palace he wants to establish. [CLS] additional approval could be met at the end of the year of 2008 compared with a bad deficit of 1. 2 billion euros (4. 06 billion euros). [CLS] it was a happy move, the play never still never begun, and three colours that put it tough on the wrist. [CLS] " for all primary medical patients monitored by statne [CLS]

PC, (32, 3), $\varepsilon = 10^{-3}$, -
PPL = 66.00, $H = 4.254$.

[CLS] allen made 27 straight saves after retiring his fifth straight shutout. [CLS] the brazilian star, previously schroeder becoming a spectator, was son of the red bull jose ronaldo santoro, who has repeatedly defended the grand prix, the argentine cradiano, with no titles. [CLS] the formal details be taken at the peak of the year, six years of sharp proportions, to 1. 2 billion euros (4. 6 billion euros). [CLS] it was just another criticism, the most recent that favre would be involved with dilili who stayed on the sept. [CLS] cnn : how do you have any conversation on the [CLS]

PC, (32, 3), $\varepsilon = 10^{-3}$, w
PPL = 52.37, $H = 4.207$.

[CLS] leader, according to a spokesman for the local and western security networks. [CLS] fox, 2 p. m. [CLS] " when we go back there ' s a very simple prospect and there ' s no plan. [CLS] you ' ll be at the usa, even crossing the san francisco bay mansion... [CLS] netilsm said second - quarter profit rose 4. 1 percent to 1. 39 billion euros (3. 3 billion dollars). [CLS] the sanctions by the united states would height president obama ' s efforts to do more to limit the spread of nuclear weapons. [CLS] rebecca blake, a research manager at wal - mart [CLS]

PC, (16, 7), $\varepsilon = 10^{-3}$, w
PPL = 48.49, $H = 4.177$.

[CLS] threat, according to the american international research organization, an industry - monitoring tank. [CLS] 30 p. m. [CLS] " with the criminal papers it ' s a little thing, because there ' s no security. [CLS] he said he had accepted the report, but added it was a " shocking document. " [CLS] in november, gm said earlier that the company had agreed to a loss of 1. 3 billion euros (2. 0 billion dollars). [CLS] the parliament also dented president nicolas sarkozy ' s plan to become president and rejected the participation of eu satellites. [CLS] it ' s a lot like the absurdity of [CLS]

VP

ODE, warp-aware, $n = 128$
PPL = 138.83, $H = 4.338$.

[CLS] and friendship, and as a democratic leadership in the aftermath of a feit conservative political movement last month marking its third anniversary to global unemployment boom. [CLS] los angeles, march 30 (upi) - - brian o ' neal ' s back lay 47 seconds with 4 : 50 left monday rallied the phoenix bulls to an 81 - 102 win over the houston bulls. [CLS] the irish soccer owner says he is considering a deal for the post - 2012 season with real madrid (3. 8 million dollars plus the price) and that it will snap up funds. [CLS] if his discrecupncy is a ticket there is a serious theat [CLS]

PC, (32, 3), $\varepsilon = 0.3$, wd
PPL = 77.02, $H = 4.204$.

[CLS]ton, who brings in both suffocation and insurance damages in the divorce of the baby, mourned the woman. [CLS] " this is the final game, " australian john john told sport, as he struggled to end the hard over team for the top spot of the schoolboy, 12 - man field. [CLS] tshlo ' s son is now the founding coach of myspace. [CLS] meanwhile, the country ' s top commissioner for information, mr suzajanh, accused his wife, abdairi ghaung, of brindling. [CLS] tesco said it was talking to the firm ' s board that [CLS]

PC, (16, 7), $\varepsilon = 0.3$, wd
PPL = 70.65, $H = 4.154$.

[CLS] bracao energy. for further information about rockmark, please visit our website at www. sereprox. com. [CLS] " this is an incredible message, " said mr. kish, as he arrived to bring his tibetan russian healthy for the olympics ahead of the inauguration. [CLS] fifa officials have already warned them that their licence was overcoenaed - indicted from jonu over pensions and garmina is suspended. [CLS] he said the outcome for most criminals was not involve transpedited inquiries into mr wilson ' s arrest. [CLS] actually, pfitat does not provide anything relevant to the user ' s full - [CLS]

VE

ODE, warp-aware, $n = 128$
PPL = 195.15, $H = 4.401$.

[CLS] scientific honey report was not the current level correct on each initiative. [CLS] while congress and democrats head for the generations to effectively lengths aclimevaously regarding climate change, progress is well - made. [CLS] more than one, 210 alexandra and barlma - - whose 2003 air force governments fail - - were executed in attacks, and at least 82 more deaths were convicted. [CLS] from two more than 70m operas per day, speakers flying into the uk to search for people metiolal difficulties, such as laurahood, family and friends to find online the day when our day. [CLS] the most vulnerable person who would lose a random tax [CLS]

PC, (32, 3), $\varepsilon = 10^{-5}$, d
PPL = 190.30, $H = 4.372$.

[CLS] no weight 5 was not the current level option on each initiative. [CLS] while congress and democrats head for the generations to themselves goals acrimicaously regarding climate change, progress is well - made. [CLS] more than one, 500 alexandra and barzee - - whose 2003 air forces governments were - - were executed in attacks, and at least 50 more deaths were arrested. [CLS] in two more than 70m operas per day, speakers pass into federal mail to search for people imiotal difficulties, such as lora chase, family and friends to find online the day when our day. [CLS] the most vulnerable person who would spend a random tax [CLS]

VE, time-conditioned

ODE, warp-aware, $n = 128$
PPL = 149.69, $H = 4.353$.

[CLS] a form of care. [CLS] minneapolis (ap) - the 23 - born harry pop actor has been given 23 years behind probation in a kidnapping he handled lured vocations. [CLS] griffithsutscher peyton made the same play. [CLS] lisa magotk, whose children all grew up in washington, n. j., and the inviltated newspaper. [CLS] sweden is just something for pizza clum at the cheese chain. [CLS] there is no quootaability to humans in any way. [CLS] but the england tradition was honoured by a host of artisttor john parcel, the little shoulders and a long sweep of arms from the glare [CLS]

Geodesic, time-conditioned

ODE, warp-aware, $n = 128$
PPL = 167.93, $H = 4.343$.

[CLS] reported to britain and belgium not be welcomed because of its large - flow costs. [CLS] cibitrgan has their clear exposure of 20 per cent, up to 171g. [CLS] in practice the company has consistently indicated it ' s too early to bury their muscle. [CLS] is this principle an irtherds ; how else will they sink into the new of indacatory warfare against irish faith? [CLS] shuhd sepiyu, the second ranking north climate scientist for many, acknowledged the swiss country was going to take these away from the ancestors and reflected off unaware " that their natural footprint was caused by an sodomion of fuel [CLS]

Degenerate low-entropy sample

VE (tc), PC, (16, 7), $\varepsilon = 10^{-2}$, –
PPL = 1.20, $H = 0.000$.

.....